

# Calcium-loaded hydrophilic hypercrosslinked polymers for extremely high defluoridation capacity via multiple uptake mechanisms

Thomas J. Robshaw, Alex M. James, Deborah B. Hammond, Jake Reynolds, Robert Dawson and Mark D. Ogden

## Supporting Information

### Table of Contents

Diagram of dynamic experiment setup	2
Photographs of polymer networks	2
Scanning electron micrographs of polymer networks	3
Calculations for Ca-loading %	5
FT-IR spectra and interpretation	7
Solid-state NMR experimental and spectra	12
Quinonoid formation within the networks	15
Powder X-ray diffractograms	15
Determination of mechanism of CaCO <sub>3</sub> formation in the networks	18
X-ray photoelectron spectra and interpretation	18
N <sub>2</sub> sorption measurements	23
Determination of protonation constants	23
Photographs of aqueous suspensions of polymers	24
Fluoride uptake studies, including pH/zeta potential dependence	27
Models used for isotherm data	28
Comparison of polymer fluoride uptake capabilities to the literature	30
Determination of release of OH <sup>-</sup> and Ca <sup>2+</sup> from networks during fluoride uptake	31
Static kinetic data and modelling	31
Dynamic breakthrough data and modelling	35
Selectivity and competition effects via ion chromatography analysis	36
Defluoridation performance of the polymers over several cycles	38
References	38

## Diagram of dynamic experiment setup

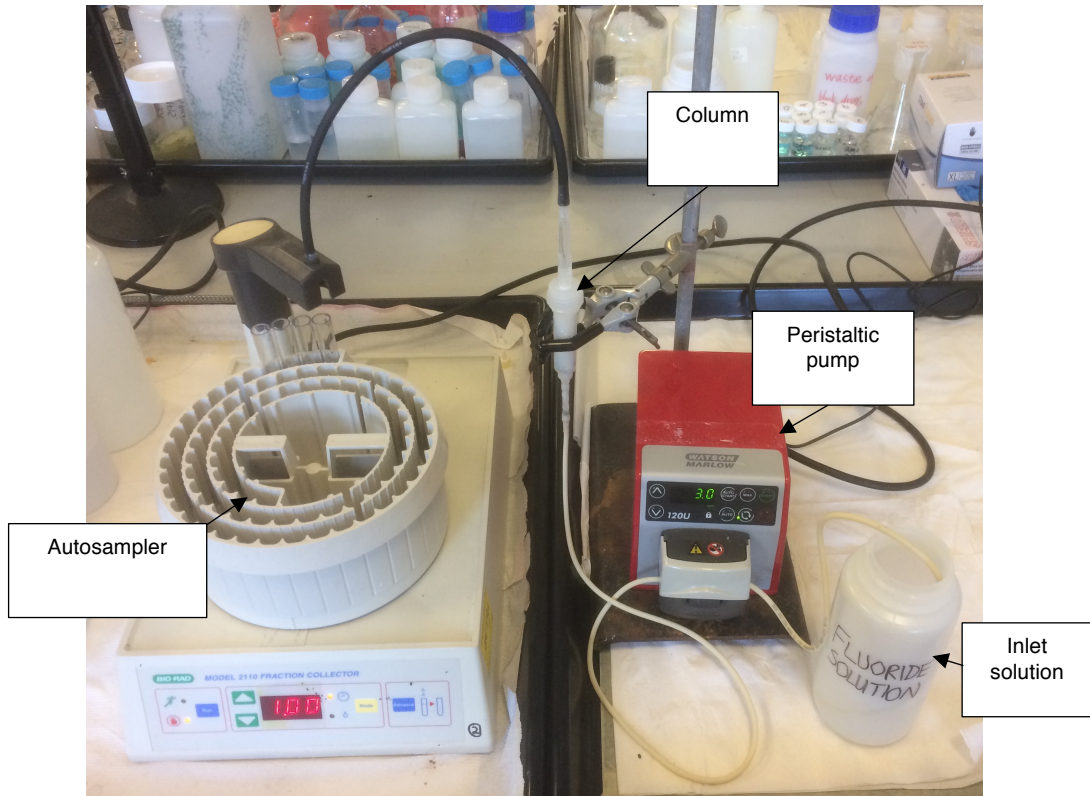


**Figure S1.** Photograph of apparatus used for reverse-flow dynamic column experiment.

## Photographs of polymer networks



**Figure S2.** Photograph of HHCP1 (left), HHCP1-Ca (centre) and HHCP1, NaOH-treated (right).



**Figure S3.** Photograph of HHCP2 (left), HHCP2-Ca (centre) and HHCP2, NaOH-treated (right).



**Figure S4.** Photograph of HCP1 (left), HCP1, Ca(OH)<sub>2</sub> treated (centre) and HHCP2, NaOH-treated (right).

### Scanning electron micrographs of polymer networks

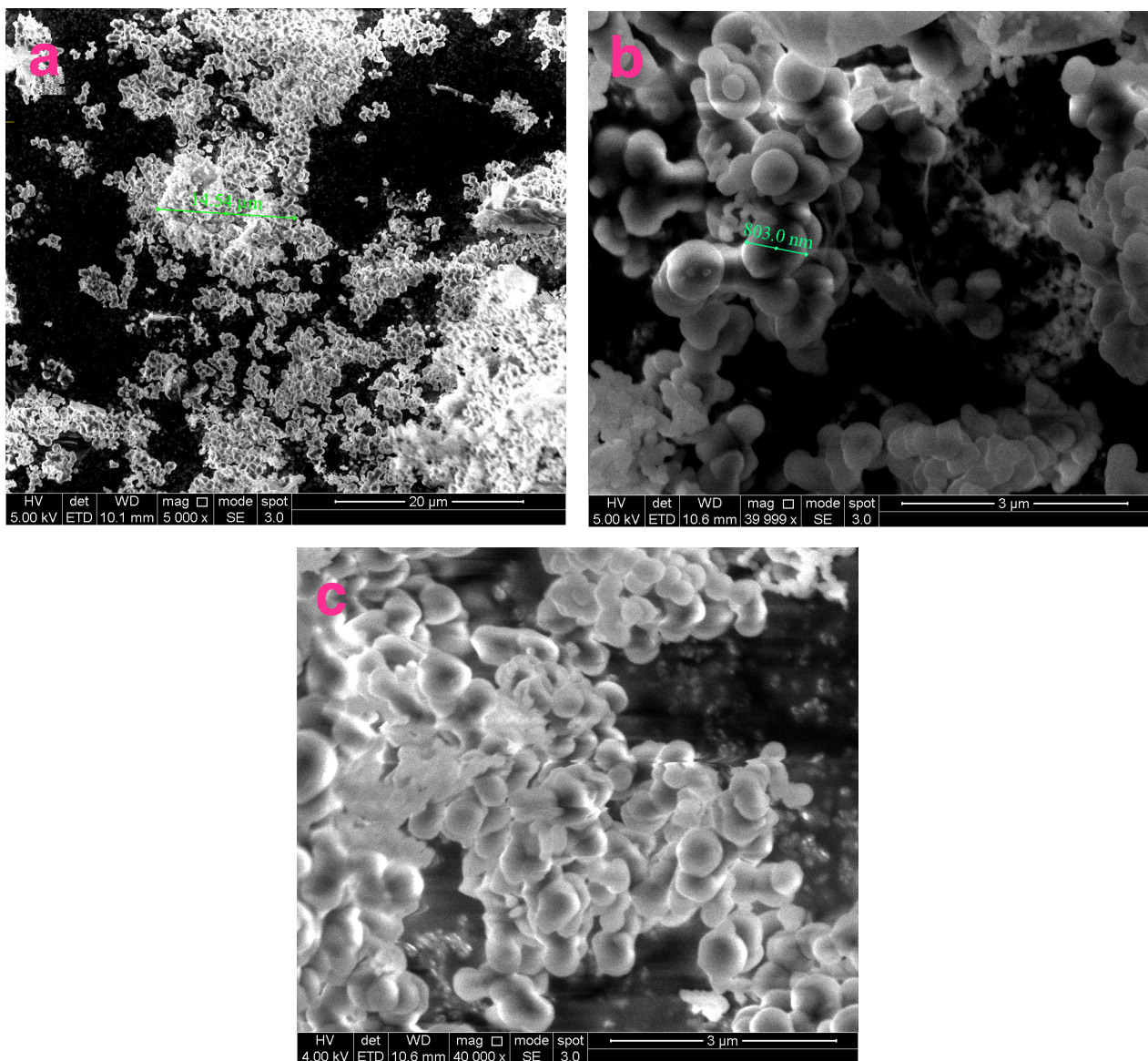


**Figure S5.** (a) HHCP1 at low magnification. Measured diameter = 14.54 μm. (b) HHCP1 at high magnification. Measured diameter = 803.0 nm. (c) HHCP1-Ca at high magnification.

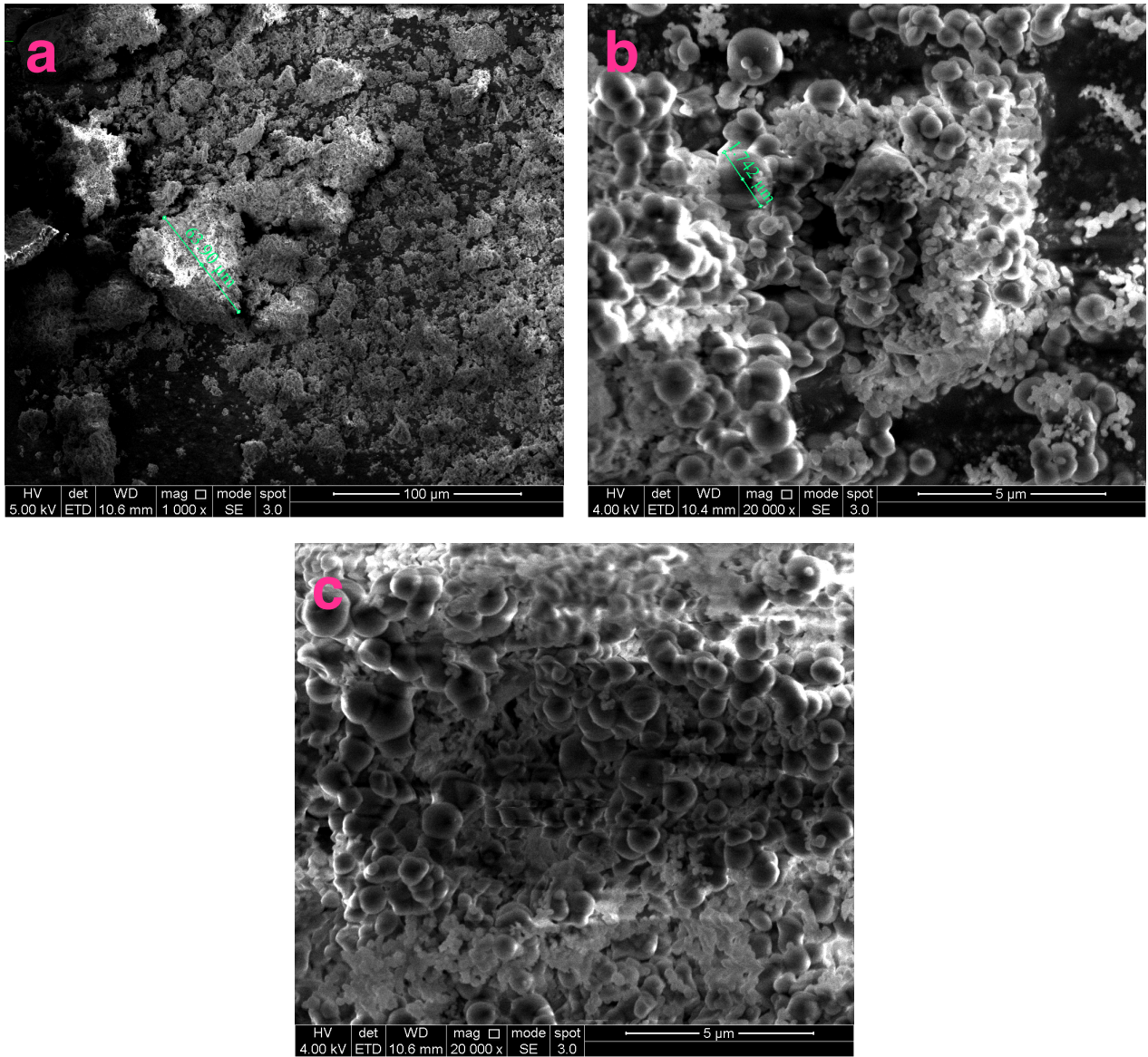


**Figure S6.** (a) HHCP2 at low magnification. Measured diameter = 63.90 μm. (b) HHCP2 at high magnification. Measured diameter = 1.742 μm. (c) HHCP2-Ca at high magnification.

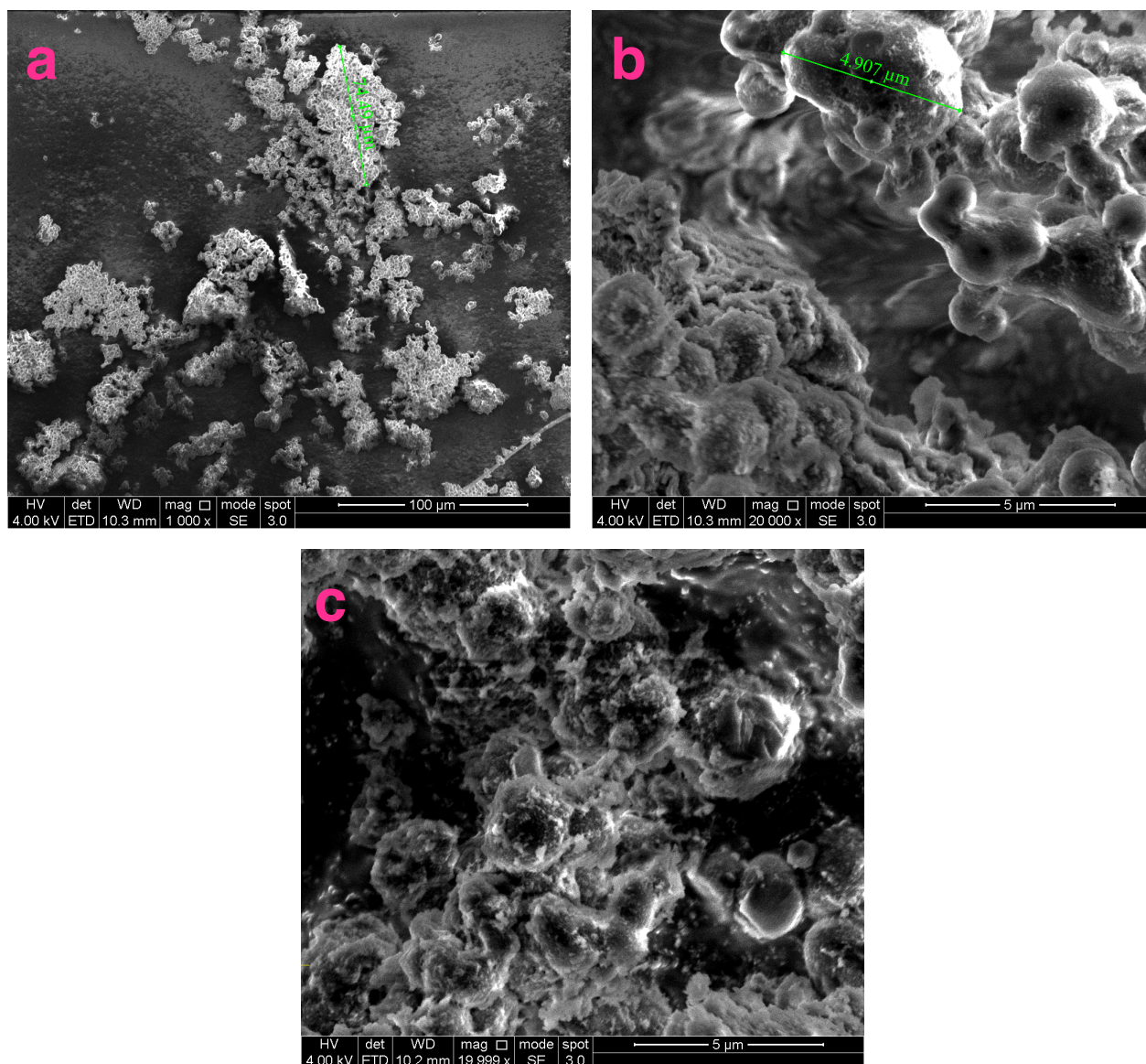


**Figure S7.** (a) HCP1 at low magnification. Measured diameter = 74.49 μm. (b) HCP1 at high magnification. Measured diameter = 4.907 μm. (c) HCP1 + Ca(OH)<sub>2</sub> at high magnification.

### Calculations for theoretical Ca-loading

The theoretical C and H mass % for the polymers shown in Table 1, main article, are based on full crosslinking occurring at every available aromatic carbon in each biphenol unit. Given the differences between theoretical and actual data, these are clearly not realistic structures to base the theoretical maximum Ca-loading capacities on. However, we can add the following modifiers to the theoretical structure: 1. Each HHCP1 biphenol unit includes two partially-reacted crosslinkers. 2. Each HHCP2 unit has four partially-reacted crosslinkers. 3. The Cl and N content of the polymers found in the elemental analysis is in the form of Cl<sup>-</sup> and NO<sub>3</sub><sup>-</sup> ions. This gives the following theoretical elemental mass % results (Figure S8 and Table S1), which are much closer to the actual results.

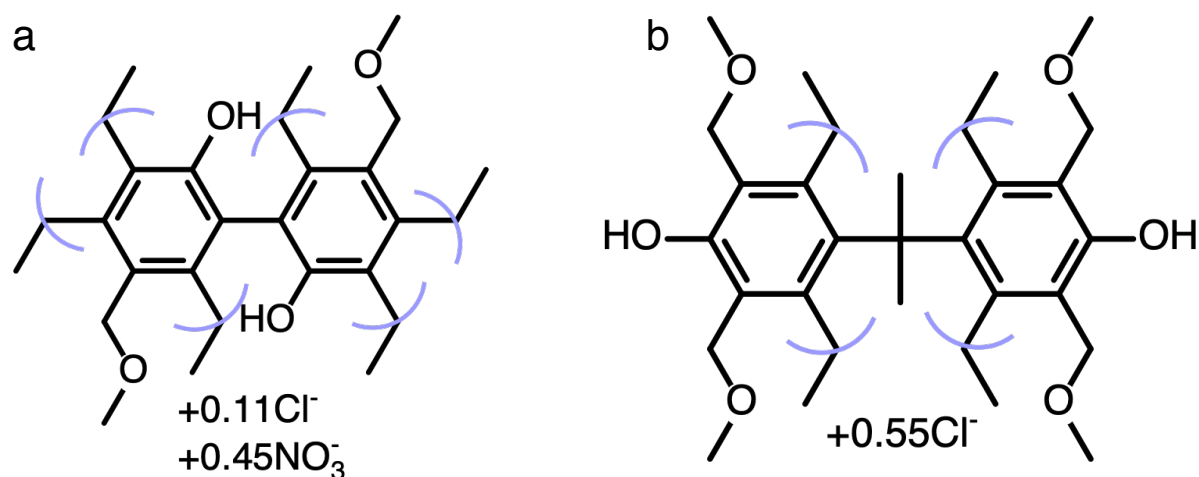


**Figure S8.** Approximate structures of biphenol units within **(a)** HHCP1 and **(b)** HHCP2, based on elemental analysis data (Table 1, main article).

**Table S1.** Approximate theoretical elemental composition of HHCP1 and HHCP2, based on the structures proposed in Figure S8. All elements are in units of mass %.

Network	C	H	O	Cl	N
HHCP1 (theoretical)	66.7	5.27	25.0	1.14	1.84
HHCP1 (actual)	69.3 ± 0.8	5.33 ± 0.14	Not measured	1.16 ± 0.13	1.84 ± 0.02
HHCP2 (theoretical)	67.0	7.15	21.5	4.35	0
HHCP2 (actual)	65.8 ± 0.1	4.20 ± 0.02	Not measured	4.38 ± 0.16	<0.1

From Table S1, the calculated theoretical concentrations of phenolic groups in the materials are 5.85 mmol·g<sup>-1</sup> for HHCP1 (calculated for C<sub>19</sub>H<sub>18</sub>O<sub>5.35</sub>N<sub>0.45</sub>Cl<sub>0.11</sub>) and 4.47 mmol·g<sup>-1</sup> for HHCP2 (calculated for C<sub>25</sub>H<sub>32</sub>O<sub>6</sub>Cl<sub>0.55</sub>), which are close to the experimental values of 6.34 and 4.57 mmol·g<sup>-1</sup>. It should be noted that these structures do not account for dehydrogenation and quinonoid formation, or the fact that the polymers immediately start equilibrating with atmospheric gases (CO<sub>2</sub> and H<sub>2</sub>O) on exposure to the air [1], which would both affect elemental analysis results. However, we considered them reasonable models to base Ca-loading efficiency on.

Assuming that Ca-loading occurs by the exchange of phenolic protons for -CaOH groups [2], the fully exchanged polymers would exhibit Ca mass % of 17.6 for HHCP1-Ca (calculated for C<sub>19</sub>H<sub>18</sub>O<sub>7.35</sub>Ca<sub>2</sub>N<sub>0.45</sub>Cl<sub>0.11</sub>) and 14.3 for HHCP2-Ca (calculated for C<sub>25</sub>H<sub>32</sub>O<sub>8</sub>Ca<sub>2</sub>Cl<sub>0.55</sub>).

Assuming that Ca-loading is only possible for half of the phenolic protons, the polymers would exhibit Ca mass % of 10.0 for HHCP1-Ca (calculated for C<sub>19</sub>H<sub>18</sub>O<sub>6.35</sub>CaN<sub>0.45</sub>Cl<sub>0.11</sub>) and 7.92 for HHCP2-Ca (calculated for C<sub>25</sub>H<sub>32</sub>O<sub>7</sub>CaCl<sub>0.55</sub>). The actual Ca mass % achieved is 9.50 and 6.39 (Table 1, main article). However, it is revealed in this work that a fraction of this is in the form of CaCO<sub>3</sub>. Therefore, it can be stated with reasonable confidence that the fraction of phenolic protons in the polymers that actually exchange is <50%.

## FT-IR Spectra

**Technical note:** FT-IR spectra were captured using both a KBr disc method (Perkin Elmer Spectrum 100) and attenuated total reflection (Perkin Elmer UATR2), as it was found that the former technique resulted in better peak intensity at higher wavenumbers, but the latter gave better resolution in the quinonoid stretching region (1600 – 1700  $\text{cm}^{-1}$ ). All peak assignments are based on KBr disc spectra and we do not make any direct comparisons or deductions based on comparison of the spectra of different polymers run on different instruments.

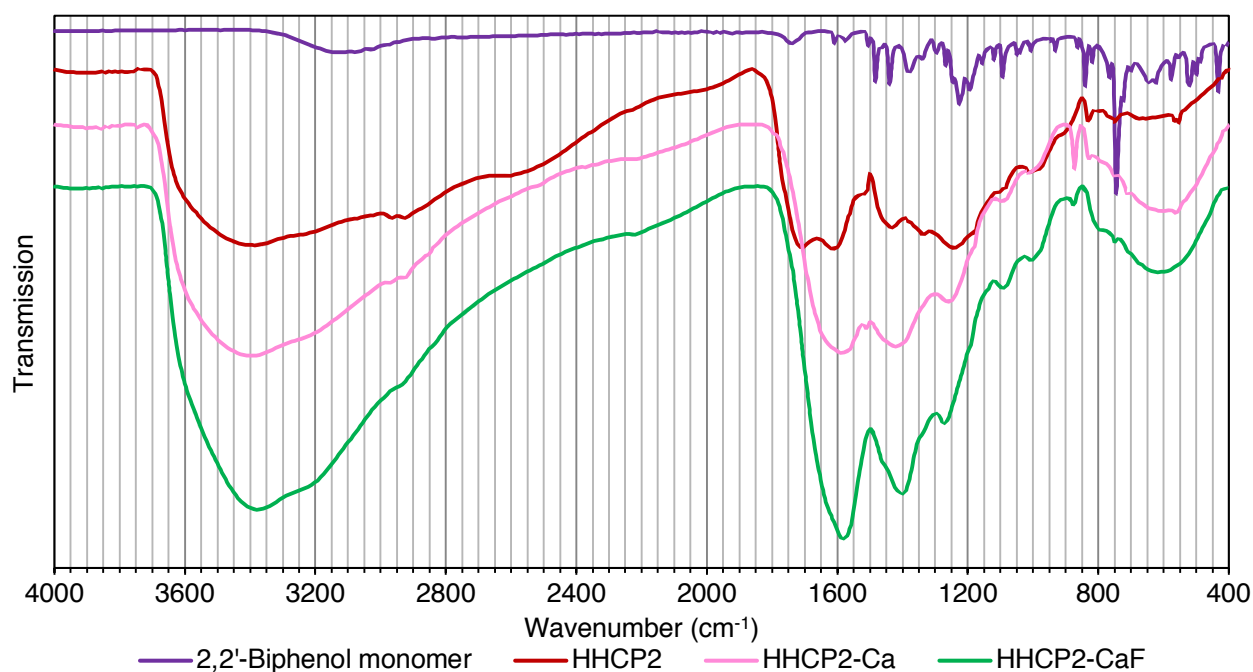


**Figure S9.** FTIR spectra of 2,2'-biphenol, HHCP1, HHCP1-Ca and HHCP1-Ca after treatment with 500  $\text{mg}\cdot\text{L}^{-1}$  fluoride (KBr disc).

**Table S2.** Peak assignments for 2,2'-biphenol, HHCP1, HHCP1-Ca and HHCP1-Ca after treatment with 500 mg·L<sup>-1</sup> fluoride.

Sample	Wavenumber (cm <sup>-1</sup> )	Assignment
2,2'-biphenol monomer	3140	O-H st.
	3025	Ar C-H st.
	1735	C=O st. (keto tautomerism)
	1610, 1570 and 1510	Combination bands
	1480, 1440 and 1380	Ar C=C st.
	1225	Ar C-O st.
	1195	Ar C-O-H st.
	1090	Ring breathing
	840 and 745	Ar C-H bend (ortho-substituted)
	640	sp <sup>2</sup> C-H bend (cis alkene, keto tautomerism)
HHCP1	3400	O-H st. (with H-bonding)
	2960 and 2920	sp <sup>3</sup> C-H st.
	1710 and 1610	Quinonoid C=C st
	1510 and 1440	Ar C=C st.
	1340	sp <sup>3</sup> C-H bend
	1245	Ar C-O st.
	1100	C-O st. (aliphatic ether)
	1010	Ring breathing
HHCP1-Ca	830 and 750	Quinonoid C-H bend
	1595	Quinonoid st.
	1420	Ar C=C st.
	1255	Ar C-OCa st.
	870	C-O st. (CO <sub>3</sub> <sup>2-</sup> )
HHCP1-CaF	600	Ca-O
	1395	Ar C=C st.
	1270	Ar C-O st.
	610	Ca-O

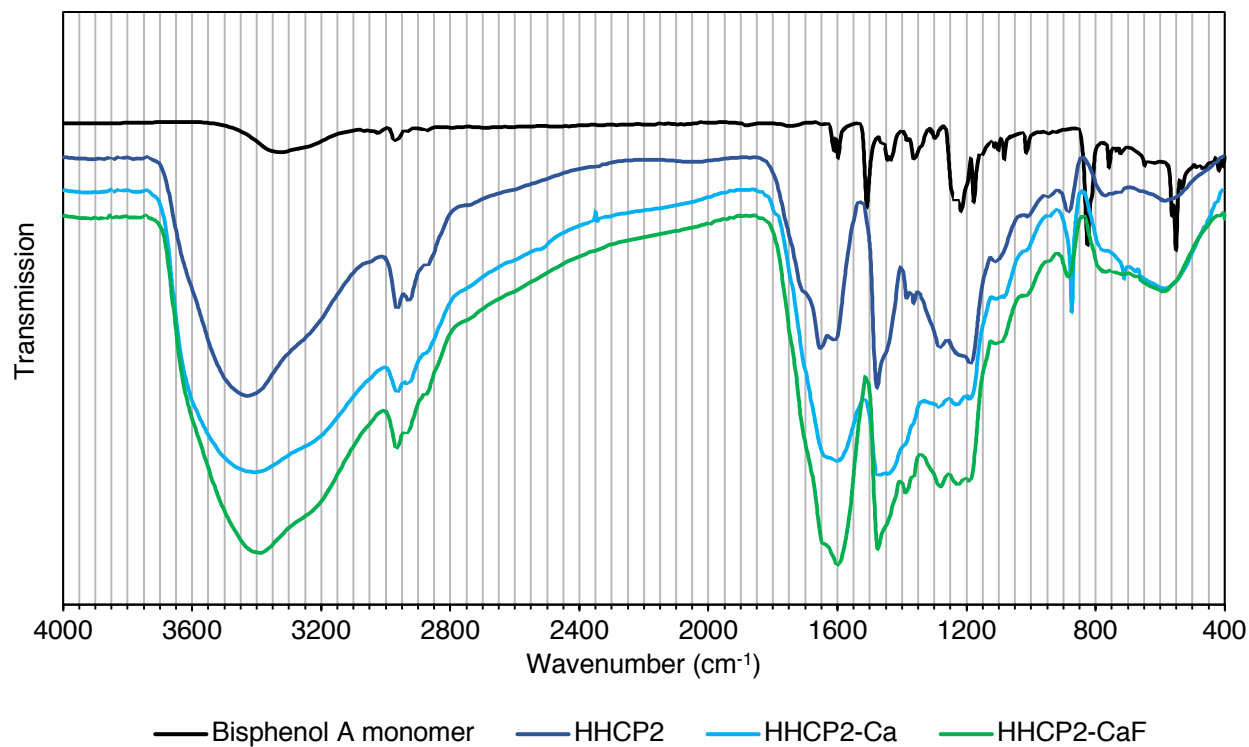


**Figure S10.** FTIR spectra of bisphenol A, HHCP2, HHCP2-Ca and HHCP2-Ca after treatment with 500 mg·L<sup>-1</sup> fluoride (KBr disc).

**Table S3.** Peak assignments for bisphenol A, HHCP2, HHCP2-Ca and HHCP2-Ca after treatment with 500 mg·L<sup>-1</sup> fluoride.

Sample	Wavenumber (cm <sup>-1</sup> )	Assignment
Bisphenol A monomer	3330	O-H st.
	3025	Ar C-H st.
	2960	sp <sup>3</sup> C-H st.
	1750 (w)	C=O st. (keto tautomerism)
	1610 and 1600	Combination bands
	1505, 1450 and 1360	Ar C=C st.
	1300	Ar C-H bend
	1215	Ar C-O st.
	1180	Ar C-O-H st.
	1080 and 1015	Ring breathing
	825	Ar C-H bend (para-substituted)
	745	Ar C-H bend (para-substituted)
	550	Ring deformation
HHCP2	3400	O-H st. (with H-bonding)
	2960 and 2920	sp <sup>3</sup> C-H st.
	1710 (shoulder), 1650 and 1605	Quinonoid C=C st.
	1480, 1380 and 1360	Ar C=C st.
	1280	Ar C-O st.
	1185	Ar C-O-H st.
	1105	C-O st. (aliphatic ether)
	880	Quinonoid C-H bend
HHCP2-Ca	875	C-O st. (CO <sub>3</sub> <sup>2-</sup> )
	710	C-O st. (CO <sub>3</sub> <sup>2-</sup> )
	590	Ca-O

**Note:** HHCP2-CaF spectrum is similar to HHCP2-Ca spectrum, due to fluoride-loading being lower than for HHCP1-Ca.

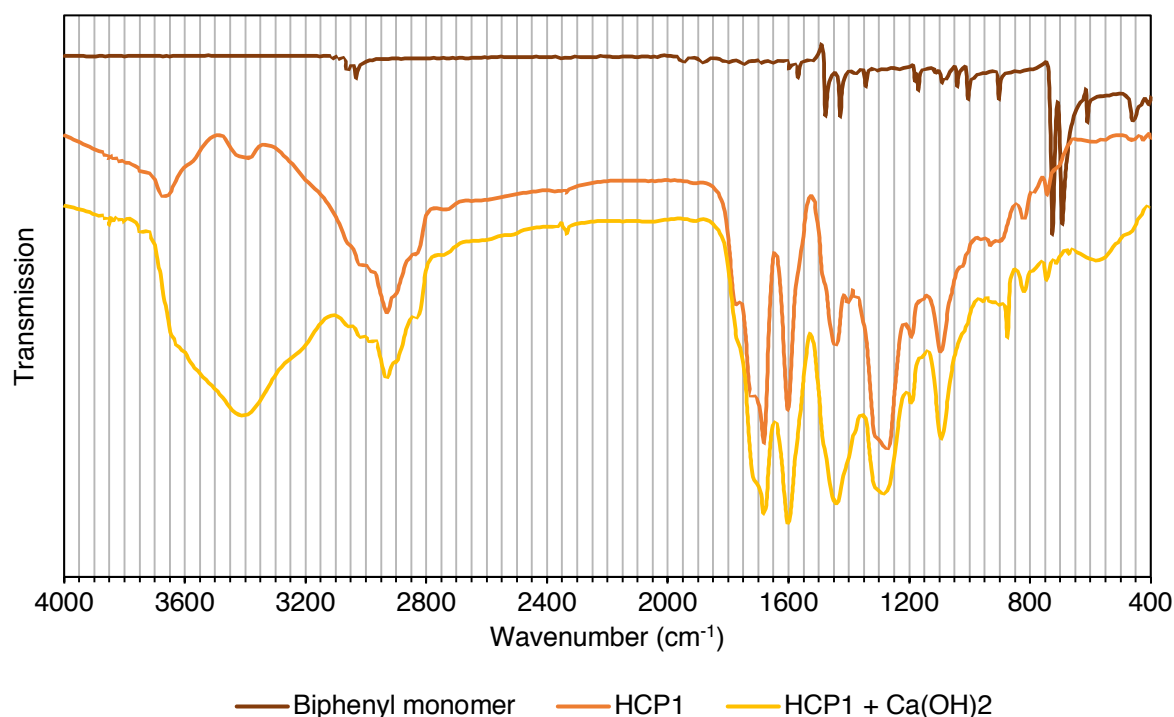


**Figure S11.** FTIR spectra of biphenyl, HCP1 and HCP1 after treatment with Ca(OH)<sub>2</sub> (KBr disc).

**Table S4.** Peak assignments for biphenyl, HCP1 and HCP1 after treatment with Ca(OH)<sub>2</sub>.

Sample	Wavenumber (cm <sup>-1</sup> )	Assignment
Biphenyl monomer	3060 and 3030	Ar C-H st.
	1600 and 1570	Combination bands
	1475, 1430 and 1340	Ar C=C st.
	1180 and 1170	Ar C-H bend
	1005	Ring breathing
	900 and 725	Ar C-H bend (monosubstituted)
	695, 610 and 460	Ring deformation
HCP1	3020	sp <sup>2</sup> C-H st.
	2930	sp <sup>3</sup> C-H st.
	2825	Aldehyde sp <sup>2</sup> C-H st.
	1680 and 1600	Quinonoid st.
	1440	Ar C=C st.
	1270	Acyl C-O st. (ester)
	1190	C-H bend
	1100	C-O st. (aliphatic ether)
	815	Quinonoid C-H bend
HCP1 + Ca(OH) <sub>2</sub>	3400	O-H st. (associated H <sub>2</sub> O)
	1400 (shoulder)	C=O st. (CO <sub>3</sub> <sup>2-</sup> )
	875	C-O st. (CO <sub>3</sub> <sup>2-</sup> )
	580	Ca-O

Assignments taken from the following references: Andersen & Brecevic [3], Galvan-Ruiz *et al.* [4], Ni & Ratner [5], Steele & Lippincott [6], Ullah *et al.* [7] and Vinodh *et al.* [8].

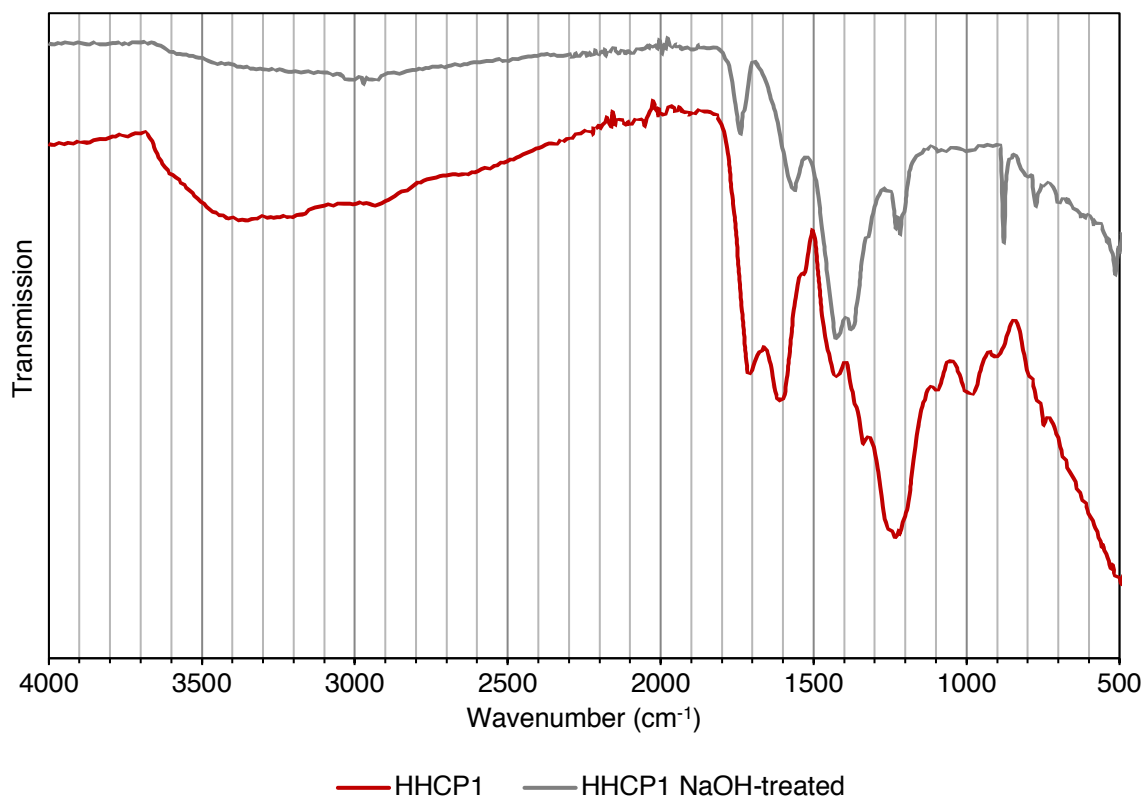


**Figure S12.** FTIR spectra of HHCP1 before and after treatment with 3 M NaOH (ATR).

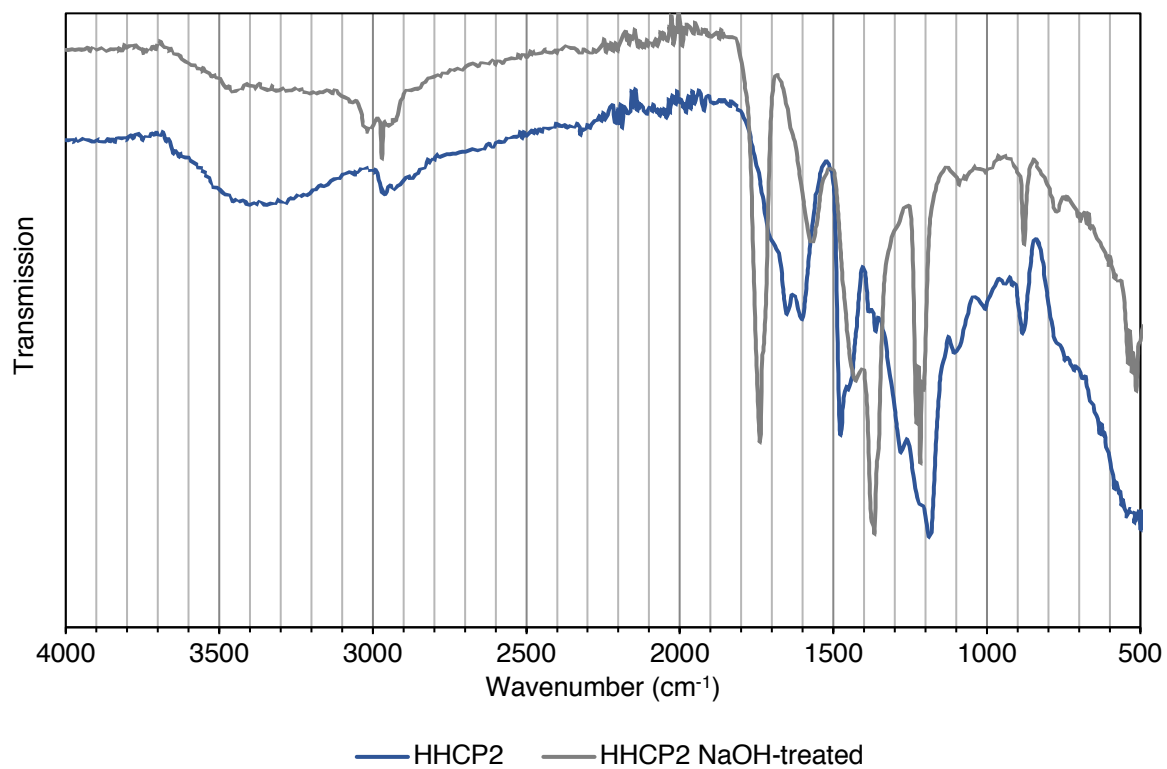


**Figure S13.** FTIR spectra of HHCP2 before and after treatment with 3 M NaOH (ATR).

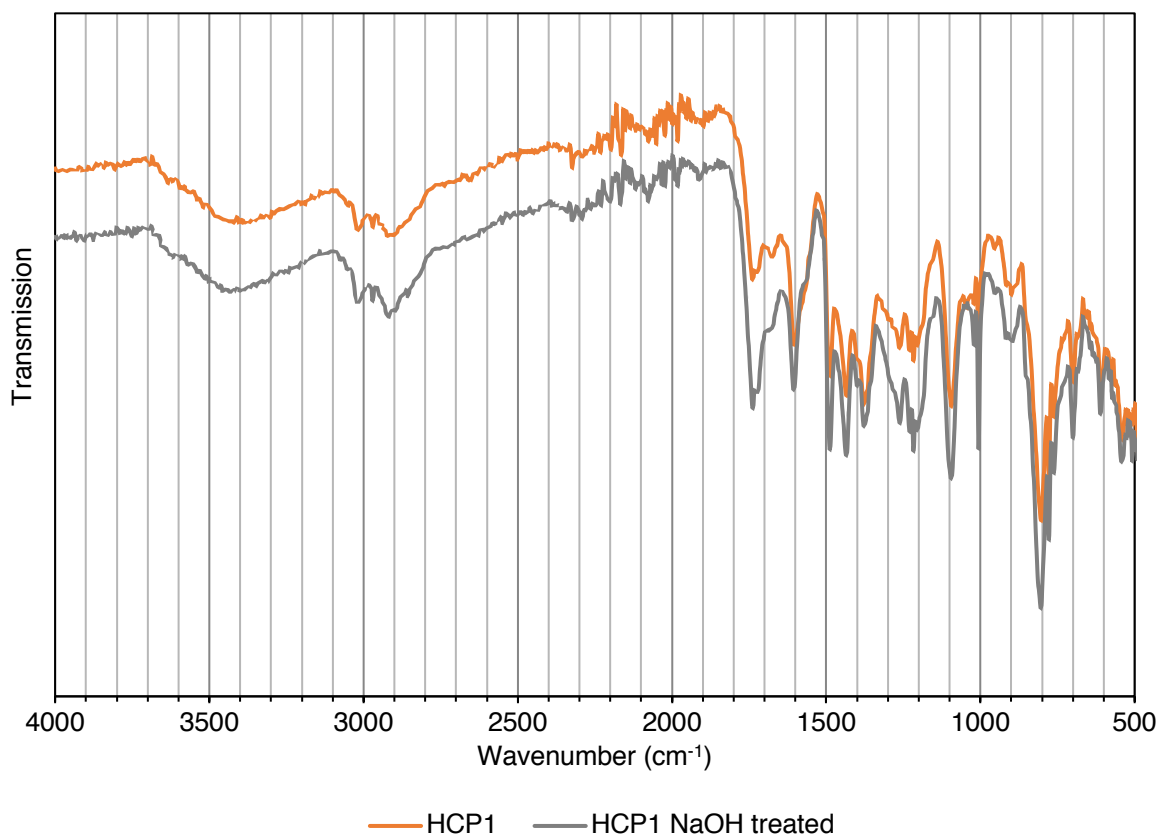


**Figure S14.** FTIR spectra of HCP1 before and after treatment with 3 M NaOH (ATR).

## Solid state NMR

### *Experimental parameters*

Solid-State NMR samples were packed into 4 mm zirconia rotors and transferred to a Bruker Avance III HD spectrometer. 1D  $^1\text{H}$ - $^{13}\text{C}$  cross-polarisation magic angle spinning (CP/MAS) NMR experiments were measured at 125.76 MHz (500.13 MHz  $^1\text{H}$ ) at a MAS rate of 10.0 kHz. The  $^1\text{H}$   $\pi/2$  pulse was 3.4  $\mu\text{s}$ , and two-pulse phase modulation (TPPM) decoupling was used during the acquisition. The Hartmann-Hahn condition was set using hexamethylbenzene. The spectra were measured using a contact time of 2.0 ms. The relaxation delay  $D_1$  for each sample was individually determined from the proton  $T_1$  measurement ( $D_1 = 5 \times T_1$ ). Samples were collected until sufficient signal to noise was observed, typically greater than 256 scans. The values of the chemical shifts are referred to tetramethylsilane.

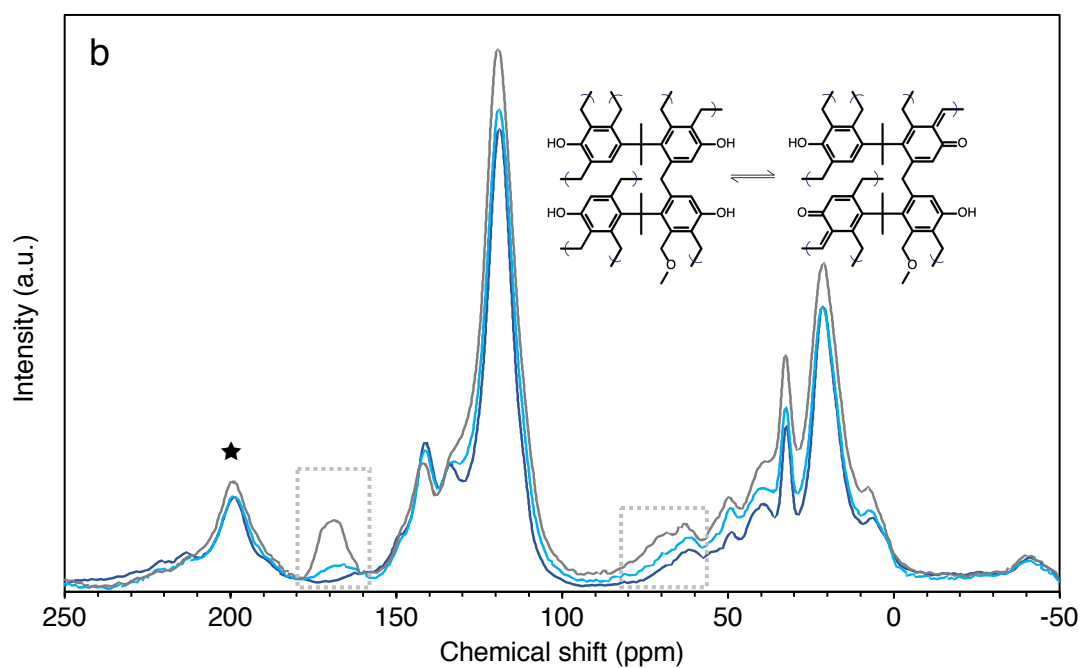
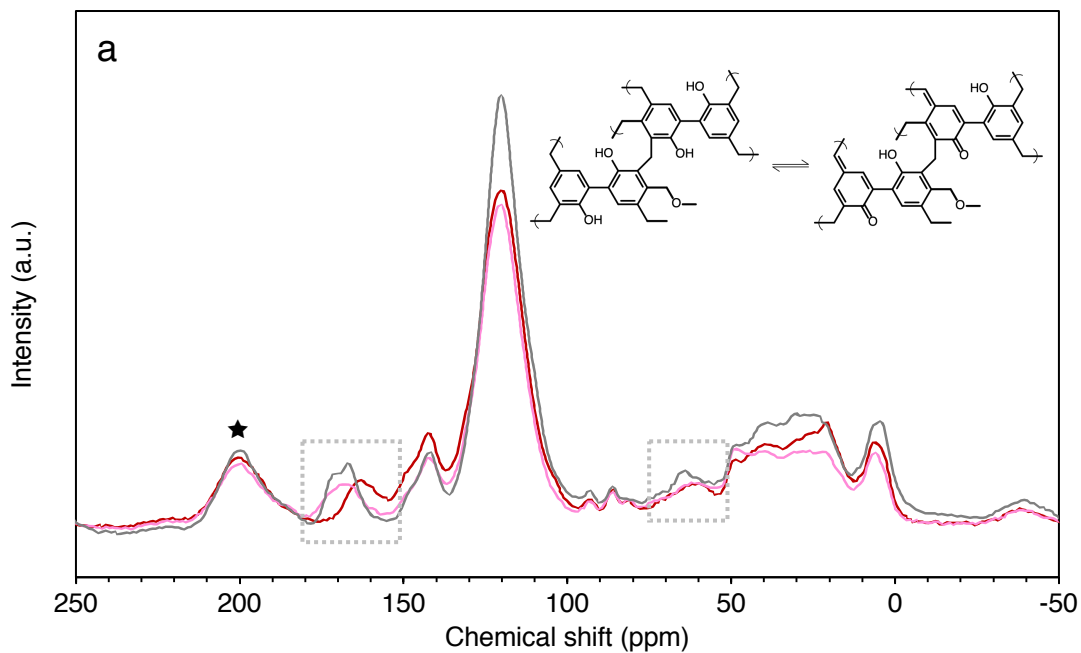


**Figure S15. (a)** Solid state NMR spectrum of 2,2'-biphenol-based polymer networks. Red line = HHCP1. Pink line = HHCP1-Ca. Grey line = HHCP1-Na. **(b)** Solid state NMR spectrum of bisphenol A-based polymer networks. Dark blue line = HHCP2. Light blue line = HHCP2-Ca. Grey line = HHCP2-Na. Regions of spectral change are highlighted. ★ = spinning side bands.

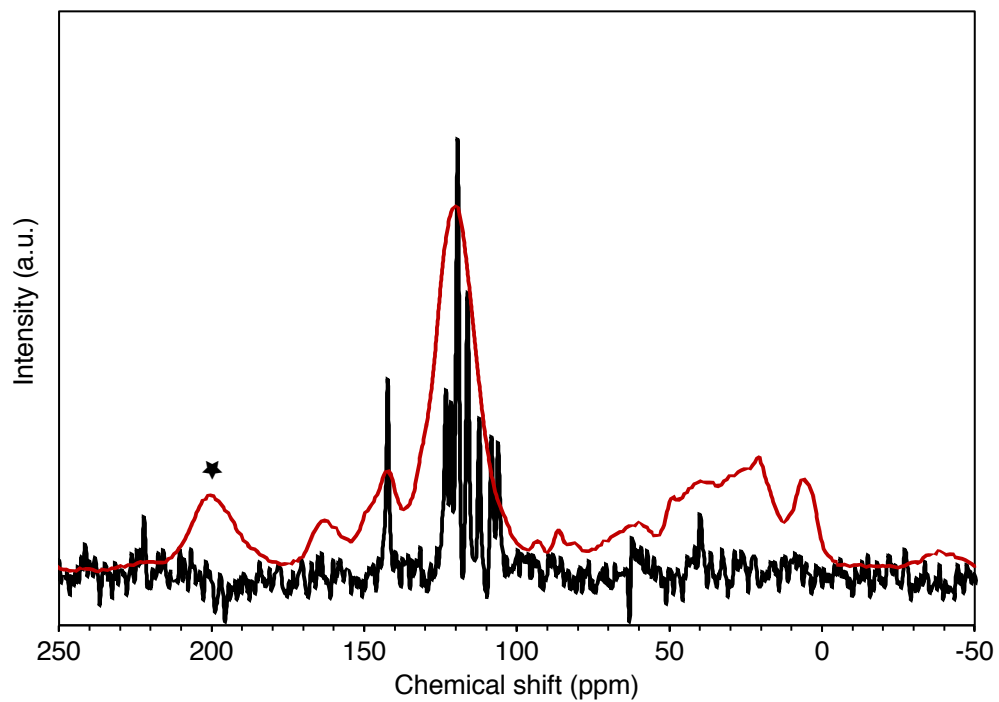


**Figure S16.** Solid state NMR spectra of 2,2'-biphenol monomer (black line) and HHCP1 (red line). ★ = spinning side band.

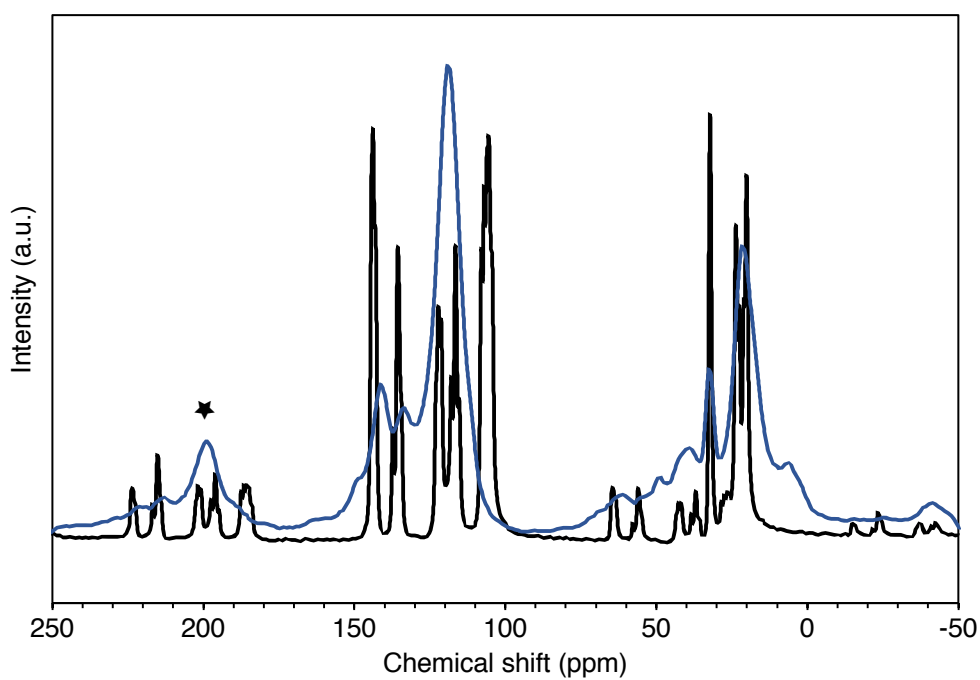


**Figure S17.** Solid state NMR spectra of bisphenol A monomer (black line) and HHCP1 (blue line). ★ = spinning side band.

## Quinonoid formation within the networks

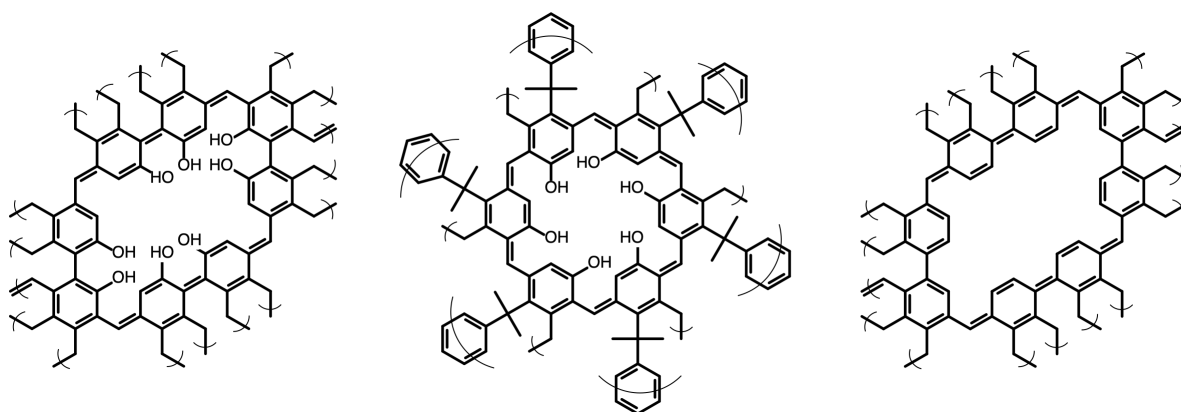


**Figure S18.** Potential quinonoid formation in HHCP1 (left), HHCP2 (centre) and HCP1 (right).

## Powder X-Ray Diffractograms

In the following diffractograms,  $\blacklozenge$  =  $\text{CaCO}_3$  (vaterite) and  $\square$  =  $\text{CaF}_2$  (fluorite).

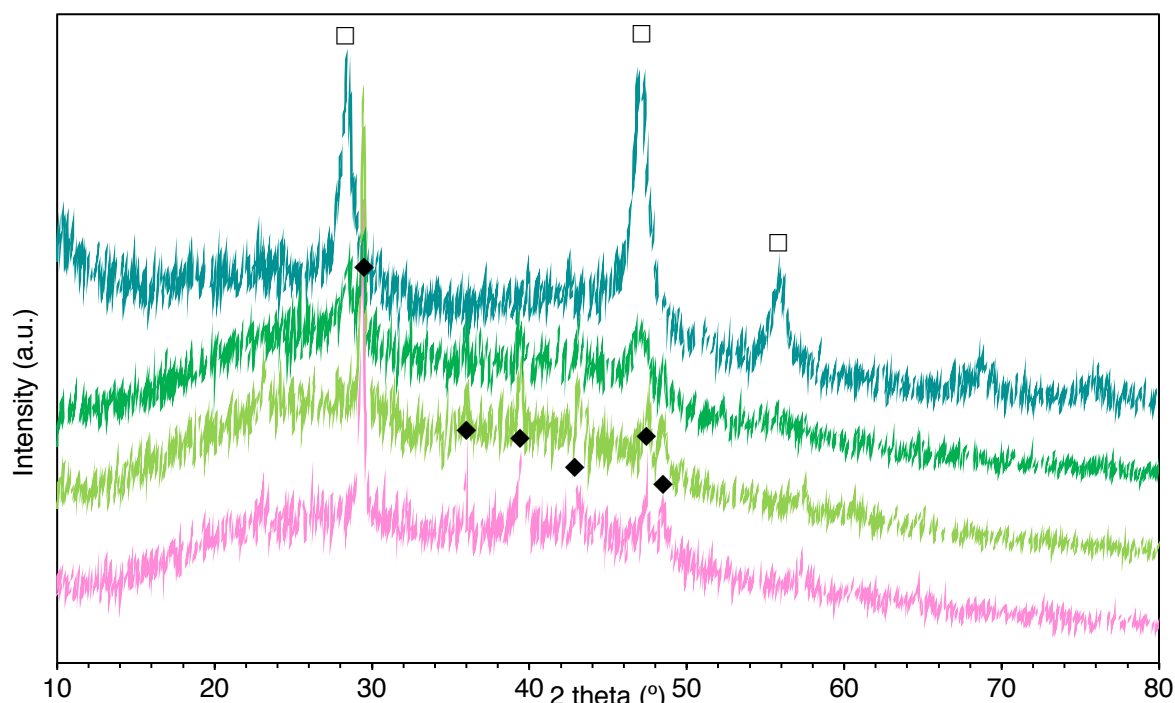


**Figure S19.** Samples of HHCP1-Ca at various process stages. **Pink line** = no further treatment. **Yellow-green line** = after contact with  $100 \text{ mg}\cdot\text{L}^{-1}$  fluoride solution. **Green line** = after contact with  $400 \text{ mg}\cdot\text{L}^{-1}$  fluoride solution. **Green-blue line** = after contact with  $2000 \text{ mg}\cdot\text{L}^{-1}$  fluoride solution (all fluoride solutions made from NaF).

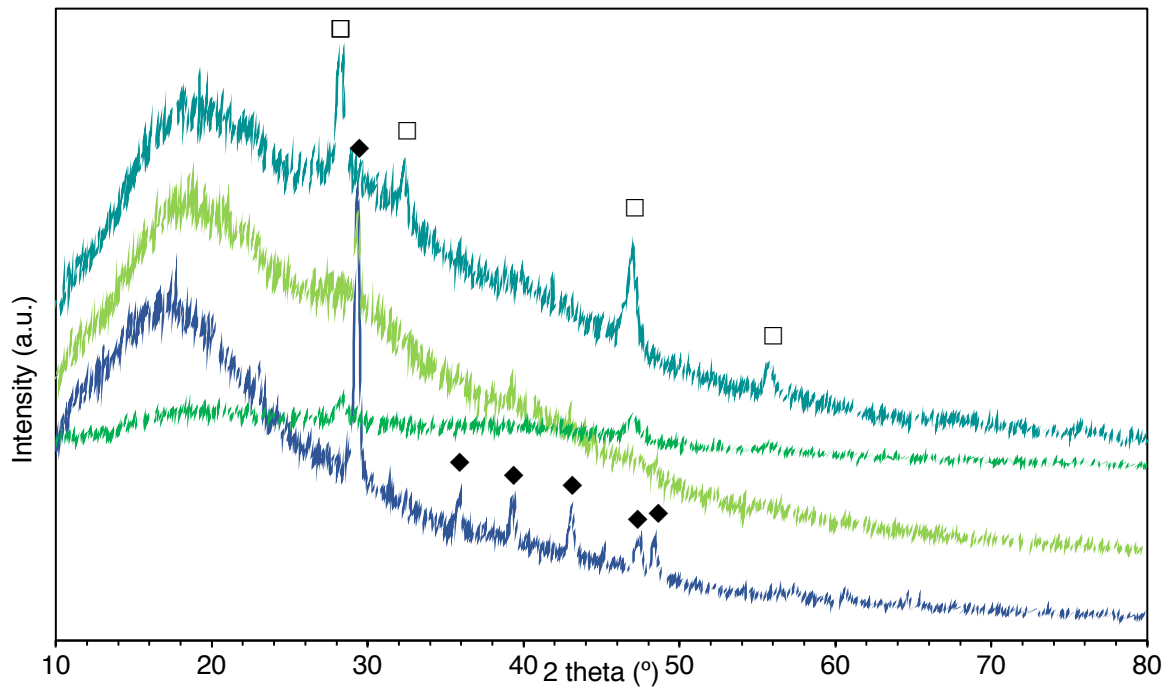


**Figure S20.** Samples of HHCP2-Ca at various process stages. **Blue line** = no further treatment. **Yellow-green line** = after contact with 100 mg·L<sup>-1</sup> fluoride solution. **Green line** = after contact with 400 mg·L<sup>-1</sup> fluoride solution. **Green-blue line** = after contact with 2000 mg·L<sup>-1</sup> fluoride solution (all fluoride solutions made from NaF).

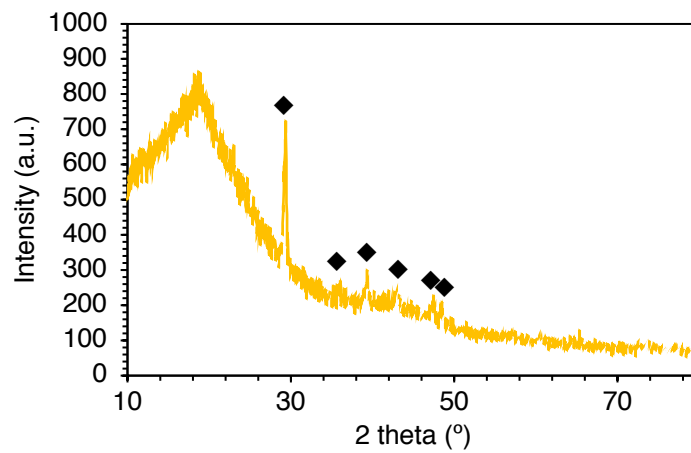


**Figure S21.** HCP1 after attempted Ca-loading with Ca(OH)<sub>2</sub>.

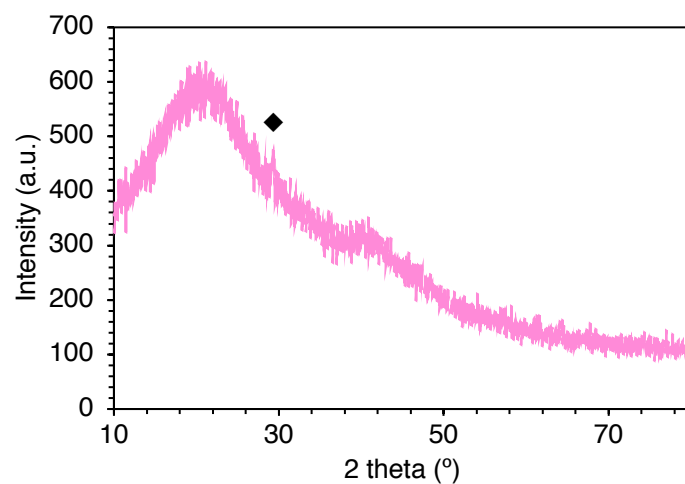


**Figure S22.** HHCP1-Ca, made by alternative procedure, whereby a sample of HHCP1 was vacuum-dried, then immediately contacted with  $\text{Ca}(\text{OH})_2$  solution, then left exposed to the atmosphere for 24 hr.

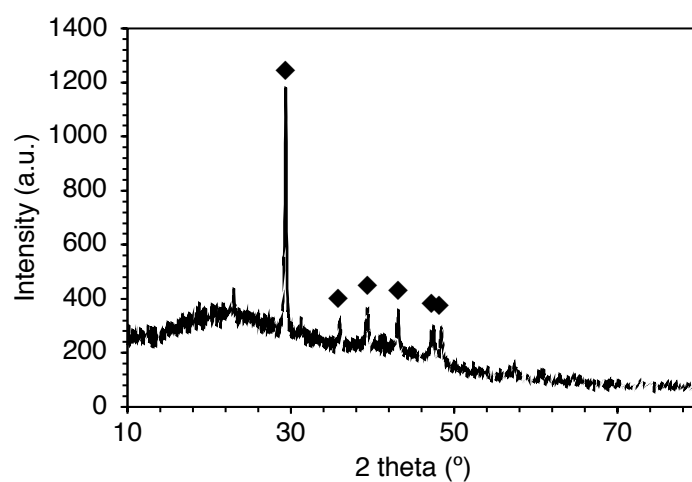


**Figure S23.** HHCP1-Ca, after contact with mixed anions solution ( $1.0 \text{ mM F}^-$ ,  $\text{Cl}^-$ ,  $\text{Br}^-$ ,  $\text{I}^-$ ,  $\text{NO}_3^-$ ,  $\text{SO}_4^{2-}$ ,  $\text{PO}_4^{3-}$  and  $\text{CO}_3^{2-}$ ).

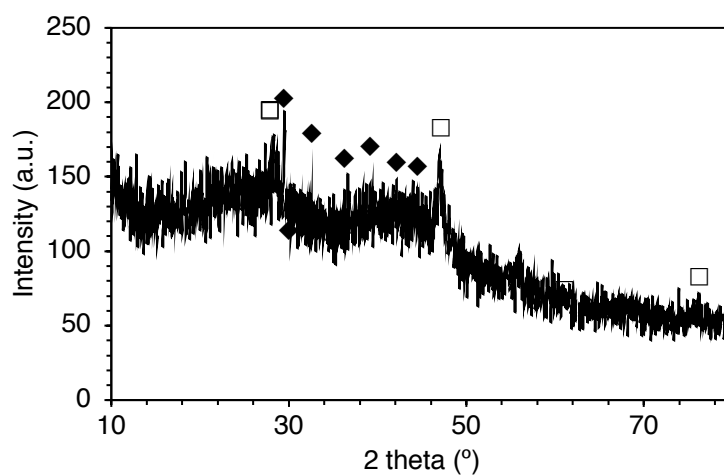


**Figure S24.** HHCP1-Ca, after contact with  $2000 \text{ mg}\cdot\text{L}^{-1}$  fluoride solution, then attempted regeneration with  $1 \text{ M NaOH}$  solution.

## Determination of mechanism of CaCO<sub>3</sub> formation in the networks

Two samples of HHCP1-Ca were compared. The first was made as described in the main article, by allowing the HHCP1 sample to equilibrate with atmospheric gases for 24 hr before Ca(OH)<sub>2</sub> contact. The sample was washed and dried in the vacuum oven, again as described in the main article, then immediately (within 10 min) was analysed by PXRD. This produced the diffractogram seen in Figure S19. The second sample was placed in the vacuum oven for 24 hr, prior to Ca-loading, then was removed and immediately (within 2 min) contacted with Ca(OH)<sub>2</sub> solution, with the sample vessel being kept sealed throughout the process to eliminate interference from atmospheric CO<sub>2</sub>. The sample was washed and dried in the vacuum oven, as previously described, then immediately (within 10 min) was analysed by PXRD, which resulted in a completely amorphous spectrum. The sample of HHCP1-Ca was then allowed to equilibrate with the atmosphere for 24 hr, before it was again analysed by PXRD. This produced the spectrum seen in Figure S22, which is almost completely amorphous, with only the major vaterite peak at ~29° being weakly visible. From these data, we concluded that the dominant formation mechanism was the interaction of Ca<sup>2+</sup>, upon Ca(OH)<sub>2</sub> treatment, with previously adsorbed CO<sub>2</sub> molecules.

## X-Ray Photoelectron Spectra

### *Experimental parameters*

The samples were all prepared by pushing the submitted HCP and HHCP powders into indium foil.

The analyses were carried out using a Kratos Supra instrument with a monochromated aluminium source, and two analysis points per sample. The analysis area was 700 μm by 300 μm. Charge neutralisation was used throughout. The survey scans were collected between 1200-0 eV, at 1 eV energy resolution, and two 300 second sweeps. High resolution O 1s, C 1s and, where appropriate, F 1s, Fe 2p, Ca 2p, Cl 2p and N 1s scans were collected over an appropriate energy range at 0.1 eV energy resolution. Two 300 seconds sweeps were collected for C 1s, O 1s, F 1s, Cl 2p and N 1s, and four 300 seconds sweeps for Fe 2p and Ca 2p.

The data collected was calibrated in intensity using a transmission function characteristic of the instrument (determined using software from NPL) to make the values instrument-independent. The data was then quantified using theoretical Schofield relative sensitivity factors. All data was calibrated relative to a C 1s position of 285.0 eV for C-C/C-H type carbon environments.

**Table S5.** Quantification results from XPS survey scans. Data for monomers are not presented, as the analysis was unreliable, due to volatilisation.

Sample	Elemental composition (atomic %)						
	Na	F	O	N	Ca	C	Cl
HHCP1 (a)	0.1	<0.1	21.1	1.9	0.1	76.3	0.4
HHCP1 (b)	0.1	<0.1	20.8	1.8	0.1	76.8	0.4
HHCP1-Ca (a)	<0.1	<0.1	26.7	1.6	5.3	63.4	0.3
HHCP1-Ca (b)	<0.1	0.1	25.6	1.5	5.1	65.6	0.3
HHCP1-Ca after F <sup>-</sup> (400 mg·L <sup>-1</sup> ) contact (a)	<0.1	1.9	18.3	2.3	4.3	72.6	0.3
HHCP1-Ca after F <sup>-</sup> (400 mg·L <sup>-1</sup> ) contact (b)	<0.1	1.5	19.9	2.2	4.4	71.4	0.3
HHCP1-Ca after F <sup>-</sup> (2000 mg·L <sup>-1</sup> ) contact (a)	<0.1	3.2	17.3	<0.1	3.7	75.0	0.7
HHCP1-Ca after F <sup>-</sup> (2000 mg·L <sup>-1</sup> ) contact (b)	<0.1	3.1	14.4	<0.1	3.5	75.2	0.8
HHCP2 (a)	<0.1	<0.1	15.4	<0.1	<0.1	83.8	0.8
HHCP2 (b)	<0.1	<0.1	15.9	<0.1	<0.1	83.4	0.6
HHCP2-Ca (a)	<0.1	<0.1	19.7	<0.1	2.7	76.3	0.5
HHCP2-Ca (b)	<0.1	<0.1	19.2	<0.1	2.7	77.2	0.5
HHCP2-Ca after F <sup>-</sup> (400 mg·L <sup>-1</sup> ) contact (a)	<0.1	5.9	16.3	<0.1	6.2	70.8	0.6
HHCP2-Ca after F <sup>-</sup> (400 mg·L <sup>-1</sup> ) contact (b)	<0.1	5.9	16.0	<0.1	6.1	71.5	0.3
HHCP2-Ca after F <sup>-</sup> (2000 mg·L <sup>-1</sup> ) contact (a)	<0.1	9.3	15.1	<0.1	8.4	66.4	0.3
HHCP2-Ca after F <sup>-</sup> (2000 mg·L <sup>-1</sup> ) contact (b)	<0.1	9.6	15.1	<0.1	8.4	66.2	0.3
HCP1 (a)	<0.1	<0.1	6.3	<0.1	<0.1	92.2	1.4
HCP1 (b)	<0.1	<0.1	6.3	<0.1	<0.1	92.3	1.4
HCP1 + Ca(OH) <sub>2</sub> (a)	<0.1	<0.1	10.4	<0.1	0.8	87.5	1.1
HCP1 + Ca(OH) <sub>2</sub> (b)	<0.1	<0.1	8.2	<0.1	0.7	90.1	1.1

**Table S6.** Results of curve-fitting of high-resolution C 1s scans.  $\pi$ - $\pi^*$  satellites not presented. B.E. = binding energy.

Sample	Environment									
	C=C sp <sub>2</sub>		Aliphatic sp <sub>3</sub>		C-O		C=O		Carbonate	
	B.E. (eV)	Atomic %	B.E. (eV)	Atomic %	B.E. (eV)	Atomic %	B.E. (eV)	Atomic %	B.E. (eV)	Atomic %
HHCP1 (a)	284.0	33.8	285.0	31.7	286.3	20.3	288.2	9.6	290.2	3.4
HHCP1 (b)	284.0	35.7	285.0	30.9	286.4	19.1	288.2	10.1	290.2	3.0
HHCP1-Ca (a)	284.0	36.5	285.0	23.1	286.1	21.5	287.8	12.0	289.8	5.4
HHCP1-Ca (b)	284.0	38.8	285.0	21.0	286.0	21.5	287.8	12.1	289.8	5.2
HHCP1-Ca after F- (400 mg·L <sup>-1</sup> ) contact (a)	284.0	37.8	285.0	40.4	286.1	9.5	287.6	9.8	289.4	1.8
HHCP1-Ca after F- (400 mg·L <sup>-1</sup> ) contact (b)	284.0	37.7	285.0	31.3	286.0	14.5	287.6	12.1	289.4	3.1
HHCP1-Ca after F- (2000 mg·L <sup>-1</sup> ) contact (a)	284.0	35.0	285.0	31.7	286.3	20.6	287.9	8.0	289.7	2.9
HHCP1-Ca after F- (2000 mg·L <sup>-1</sup> ) contact (b)	284.0	41.1	285.0	26.1	286.1	20.5	287.8	7.8	289.8	2.9
HHCP2 (a)	284.3	53.1	285.0	23.4	285.9	14.8	286.9	4.7	288.3	4.1
HHCP2 (b)	284.3	46.7	285.0	25.3	285.9	16.3	286.8	5.7	288.0	6.0
HHCP2-Ca (a)	284.2	46.6	284.8	28.6	285.8	13.2	286.6	6.4	290.7	5.2
HHCP2-Ca (b)	284.2	49.0	284.9	22.5	285.7	13.5	286.5	7.2	287.8	7.8
HHCP2-Ca after F- (400 mg·L <sup>-1</sup> ) contact (a)	284.2	57.1	285.0	20.0	286.0	11.3	286.6	4.7	287.9	6.8
HHCP2-Ca after F- (400 mg·L <sup>-1</sup> ) contact (b)	284.3	47.7	284.8	21.7	285.7	15.7	286.6	8.4	288.0	6.6
HHCP2-Ca after F- (2000 mg·L <sup>-1</sup> ) contact (a)	284.2	40.3	284.9	23.0	285.7	16.2	286.5	8.7	287.6	11.8
HHCP2-Ca after F- (2000 mg·L <sup>-1</sup> ) contact (b)	284.3	56.4	285.2	13.4	286.1	19.8	287.0	3.7	288.0	6.8
HCP1 (a)	284.0	79.9	285.2	9.1	286.2*		4.9*		290.2	6.1
HCP1 (b)	284.0	70.8	285.3	18.4	286.3*		5.1*		290.2	5.8
HCP1 + Ca(OH) <sub>2</sub> (a)	284.1	72.7	285.2	12.2	286.4*		6.2*		289.8	8.9
HCP1 + Ca(OH) <sub>2</sub> (b)	284.1	82.9	285.1	5.2	286.2*		5.9*		290.5	5.9

\*These C-O and C=O environments could not be distinguished.

#### Technical notes:

For C 1s curve-fitting for HHCP1 and derivatives, the sp<sup>2</sup> peak was made asymmetric and allowed to be narrower than the sp<sup>3</sup> peaks, as is typical in polymeric samples. This gave sensible relative ratios of all carbons. The same practice was tried for HHCP2 and derivatives, but this gave illogical carbon ratios (only ~20% sp<sup>2</sup>). An alternative sp<sup>2</sup> curve-fitting was tried: instead of assuming a narrower asymmetric peak compared to the sp<sup>3</sup> components, it was fitted as a symmetric peak of equal width to all the other carbon components. No additional calibrations to the energy scale were made and this produced sensible carbon ratios. A narrower and more symmetrical sp<sup>2</sup> peak is commonly seen in graphene type samples and this suggests that quinonoid-formation is more prevalent in HHCP2 than HHCP1. This indeed is also suggested by the relative ratios of sp<sup>2</sup> to sp<sup>3</sup> carbons in XPS spectra and also the much lower than calculated H mass % of HHCP2 (Table S1).

The atomic % of C=C carbons for HHCP1 and HHCP2 polymers and derivatives is somewhat lower than expected, assuming the dehydrogenation and quinonoid formation

proposed by Vinodh *et al.* is occurring [8] (suggested by FT-IR data). It is possible that during the polymerisations, the  $\text{FeCl}_3$  migrates to the relatively hydrophilic pore interiors, rather than the particle surfaces, which are in contact with hydrophobic DCE. For this reason, the surface sites analysed by XPS are likely to contain more aliphatic crosslinkers and partial crosslinkers than aromatised crosslinkers.

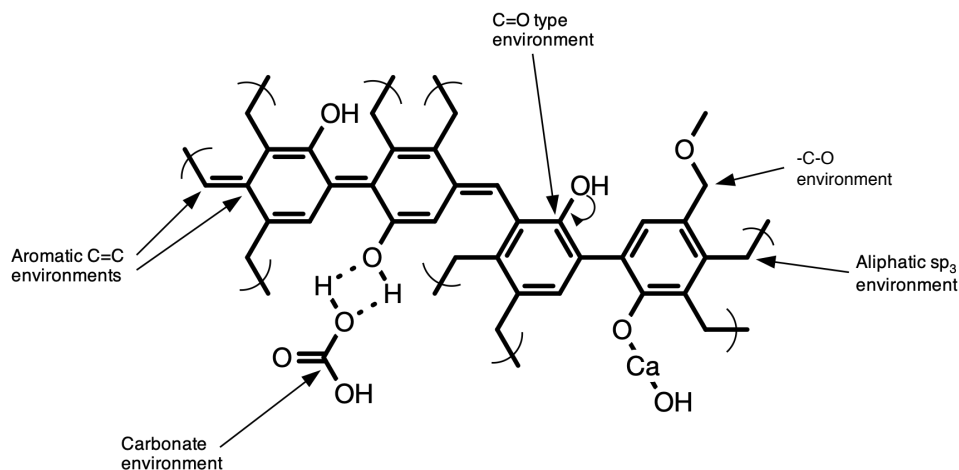


**Figure S25.** Structure of HHCP1 with assigned XPS carbon environments.

**Table S7.** Results of curve-fitting of high-resolution O 1s scans.

Sample	Environment					
	C-O-, Ca-O- and carbonate		C=O		Adsorbed water	
	B.E. (eV)	Atomic %	B.E. (eV)	Atomic %	B.E. (eV)	Atomic %
HHCP1 (a)	531.3	28.1	532.6	58.4	534.3	13.5
HHCP1 (b)	531.3	28.0	532.6	58.1	534.5	13.9
HHCP1-Ca (a)	531.0	51.4	532.5	37.9	534.3	10.7
HHCP1-Ca (b)	531.0	49.7	532.5	39.5	534.3	10.8
HHCP1-Ca after F <sup>-</sup> (400 mg·L <sup>-1</sup> ) contact (a)	530.8	52.6	532.3	42.4	533.7	5.1
HHCP1-Ca after F <sup>-</sup> (400 mg·L <sup>-1</sup> ) contact (b)	530.8	49.5	532.3	43.4	533.9	7.1
HHCP1-Ca after F <sup>-</sup> (2000 mg·L <sup>-1</sup> ) contact (a)	531.0	24.4	532.5	62.7	534.3	13.0
HHCP1-Ca after F <sup>-</sup> (2000 mg·L <sup>-1</sup> ) contact (b)	530.9	22.9	532.5	63.6	534.3	13.6
HHCP2 (a)	531.4	15.2	532.7	84.8		
HHCP2 (b)	531.5	17.2	532.7	82.8		
HHCP2-Ca (a)	531.2	30.1	532.6	69.9		
HHCP2-Ca (b)			532.2	100		
HHCP2-Ca after F <sup>-</sup> (400 mg·L <sup>-1</sup> ) contact (a)	531.3	29.0	532.6	71.0		
HHCP2-Ca after F <sup>-</sup> (400 mg·L <sup>-1</sup> ) contact (b)	531.5	30.6	532.9	69.4		
HHCP2-Ca after F <sup>-</sup> (2000 mg·L <sup>-1</sup> ) contact (a)	531.3	23.3	532.7	66.6	534.3	10.1
HHCP2-Ca after F <sup>-</sup> (2000 mg·L <sup>-1</sup> ) contact (b)			532.4	100		
HCP1 (a)			532.0	100		
HCP1 (b)			532.1	100		
HCP1 + Ca(OH) <sub>2</sub> (a)			532.0	100		
HCP1 + Ca(OH) <sub>2</sub> (b)			532.1	100		

**Table S8.** Results of curve-fitting of high-resolution Ca 2p scans.

Sample	Environment											
	RO-Ca-OH and CaCO <sub>3</sub>				CaF <sub>2</sub>				Coordinated CaX <sub>2</sub>			
	2p 3/2		2p 1/2		2p 3/2		2p 1/2		2p 3/2		2p 1/2	
	B.E. (eV)	Atom %	B.E. (eV)	Atom %	B.E. (eV)	Atom %	B.E. (eV)	Atom %	B.E. (eV)	Atom %	B.E. (eV)	Atom %
HHCP1-Ca (a)	346.9	54.2	350.7	27.0					349.5	12.5	353.0	6.3
HHCP1-Ca (b)	346.9	55.4	350.6	27.7					349.5	11.3	353.0	5.6
HHCP1-Ca after F <sup>-</sup> (400 mg·L <sup>-1</sup> ) contact (a)	347.1	66.7	350.6	33.3								
HHCP1-Ca after F <sup>-</sup> (400 mg·L <sup>-1</sup> ) contact (b)	347.0	50.3	350.5	25.1					350.0	16.4	353.5	8.2
HHCP1-Ca after F <sup>-</sup> (2000 mg·L <sup>-1</sup> ) contact (a)					348.0	66.7	351.6	33.3				
HHCP1-Ca after F <sup>-</sup> (2000 mg·L <sup>-1</sup> ) contact (b)					347.9	66.7	351.5	33.3				
HHCP2-Ca (a)	347.4	66.7	351.0	33.3								
HHCP2-Ca (b)	347.4	66.7	351.0	33.3								
HHCP2-Ca after F <sup>-</sup> (400 mg·L <sup>-1</sup> ) contact (a)					348.7	66.7	351.9	33.3				
HHCP2-Ca after F <sup>-</sup> (400 mg·L <sup>-1</sup> ) contact (b)					348.3	66.7	352.0	33.3				
HHCP2-Ca after F <sup>-</sup> (2000 mg·L <sup>-1</sup> ) contact (a)					348.5	66.7	352.0	33.3				
HHCP2-Ca after F <sup>-</sup> (2000 mg·L <sup>-1</sup> ) contact (b)					348.6	66.7	352.1	33.3				
HCP1 + Ca(OH) <sub>2</sub> (a)	347.6	66.7	351.4	33.3								
HCP1 + Ca(OH) <sub>2</sub> (b)	347.8	66.7	351.5	33.3								

**Table S9.** Results of curve-fitting of high-resolution F 1s scans.

Sample	Environment					
	CaF <sub>2</sub>		F ligand		F bridging ligand	
	B.E. (eV)	Atomic %	B.E. (eV)	Atomic %	B.E. (eV)	Atomic %
HHCP1-Ca after F <sup>-</sup> (400 mg·L <sup>-1</sup> ) contact (a)	685.0	100				
HHCP1-Ca after F <sup>-</sup> (400 mg·L <sup>-1</sup> ) contact (b)	684.8	47.0	686.6	53.0		
HHCP1-Ca after F <sup>-</sup> (2000 mg·L <sup>-1</sup> ) contact (a)	685.3	63.7	686.7	26.5	688.6	9.8
HHCP1-Ca after F <sup>-</sup> (2000 mg·L <sup>-1</sup> ) contact (b)	685.2	66.0	687.0	20.6	689.1	13.5
HHCP2-Ca after F <sup>-</sup> (400 mg·L <sup>-1</sup> ) contact (a)	685.5	83.4	687.2	16.6		
HHCP2-Ca after F <sup>-</sup> (400 mg·L <sup>-1</sup> ) contact (b)	685.7	79.8	687.3	20.2		
HHCP2-Ca after F <sup>-</sup> (2000 mg·L <sup>-1</sup> ) contact (a)	685.4	70.5	686.8	23.9	688.3	5.7
HHCP2-Ca after F <sup>-</sup> (2000 mg·L <sup>-1</sup> ) contact (b)	685.4	78.0	686.4	19.9	688.1	2.1

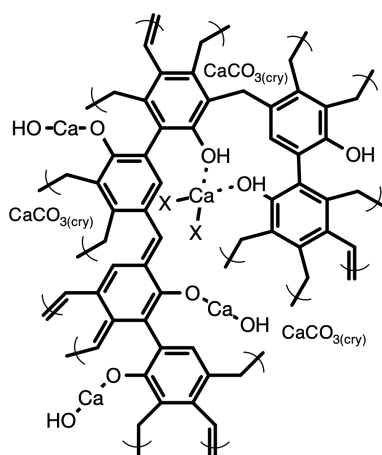


**Figure S26.** Structure of HHCP1-Ca showing low B.E. and high B.E. Ca environments. X = OH, Cl or NO<sub>3</sub>. Note that after 400 mg·L<sup>-1</sup> F<sup>-</sup> contact, the high B.E. environment becomes more electron-poor, shifting by 0.5 eV, due to the electronegativity of the F ligands.

## N<sub>2</sub> sorption measurements

**Table S10.** Calculated parameters for the polymer networks from N<sub>2</sub> sorption experiments. Sample mass ≈ 100 mg. T = 77 K.

Sample	BET surface area (m <sup>2</sup> ·g <sup>-1</sup> )	BET equation R <sup>2</sup>	Micropore volume (cm <sup>3</sup> ·g <sup>-1</sup> )	Total pore volume (cm <sup>3</sup> ·g <sup>-1</sup> )	V <sub>micro</sub> / V <sub>total</sub>	Average pore size (nm)	Median pore size (nm)
HHCP1	748 ± 5	0.9999	0.294	0.379	0.776	2.03	0.495
HHCP1-Ca	334 ± 2	0.9999	0.132	0.170	0.776	2.03	0.614
HHCP2	541 ± 4	0.9999	0.212	0.272	0.779	2.01	0.490
HHCP2-Ca	17.1 ± 0.1	0.9999	0.006	0.018	0.333	4.16	0.781
HCP1	1310 ± 1	0.9999	0.500	1.161	0.431	3.55	0.574
HCP1 + Ca(OH) <sub>2</sub>	1140 ± 1	0.9999	0.437	0.944	0.463	3.31	0.554

**Notes:** Surface areas were calculated over a P/P<sub>0</sub> range of 0.01 – 0.11 using BET equation. Micropore volume was calculated at P/P<sub>0</sub> = 0.01. Total pore volume was calculated at P/P<sub>0</sub> = 0.95.

## Determination of protonation constants

**Table S11.** pK<sub>a</sub> values determined from the three best-fitting models for HHCP1. Experimental parameters as described in the main article.

Model	Log <sub>10</sub> K <sub>1</sub>	Log <sub>10</sub> K <sub>2</sub>	Log <sub>10</sub> K <sub>3</sub>	Log <sub>10</sub> K <sub>4</sub>	R <sup>2</sup>
2 pK <sub>a</sub> s	9.24 ± 0.06	4.88 ± 0.05			0.9981
3 pK <sub>a</sub> s	10.2 ± 0.07	8.77 ± 0.04	4.73 ± 0.04		0.9995
4 pK <sub>a</sub> s	10.5 ± 0.1	9.99 ± 0.06	8.48 ± 0.05	4.86 ± 0.04	0.9997

**Table S12.** pK<sub>a</sub> values determined from the three best-fitting models for HHCP2. Experimental parameters as described in the main article.

Model	Log <sub>10</sub> K <sub>1</sub>	Log <sub>10</sub> K <sub>2</sub>	Log <sub>10</sub> K <sub>3</sub>	Log <sub>10</sub> K <sub>4</sub>	Log <sub>10</sub> K <sub>5</sub>	R <sup>2</sup>
3 pK <sub>a</sub> s	9.91 ± 0.09	9.60 ± 0.08	7.38 ± 0.11			0.9991
4 pK <sub>a</sub> s	9.93 ± 0.19	9.87 ± 0.09	8.87 ± 0.16	6.30 ± 0.14		0.9994
5 pK <sub>a</sub> s	10.1 ± 0.3	9.90 ± 0.09	9.19 ± 0.20	7.54 ± 0.12	3.33 ± 0.13	0.9996

**Note:** The 5 pK<sub>a</sub> model for HHCP1 and 6 pK<sub>a</sub> model for HHCP2 gave R<sup>2</sup> values of 0.9995 and 0.9994, but returned illogical parameters (pK<sub>a</sub>s with value of 0).

## Photographs of aqueous suspensions of polymers

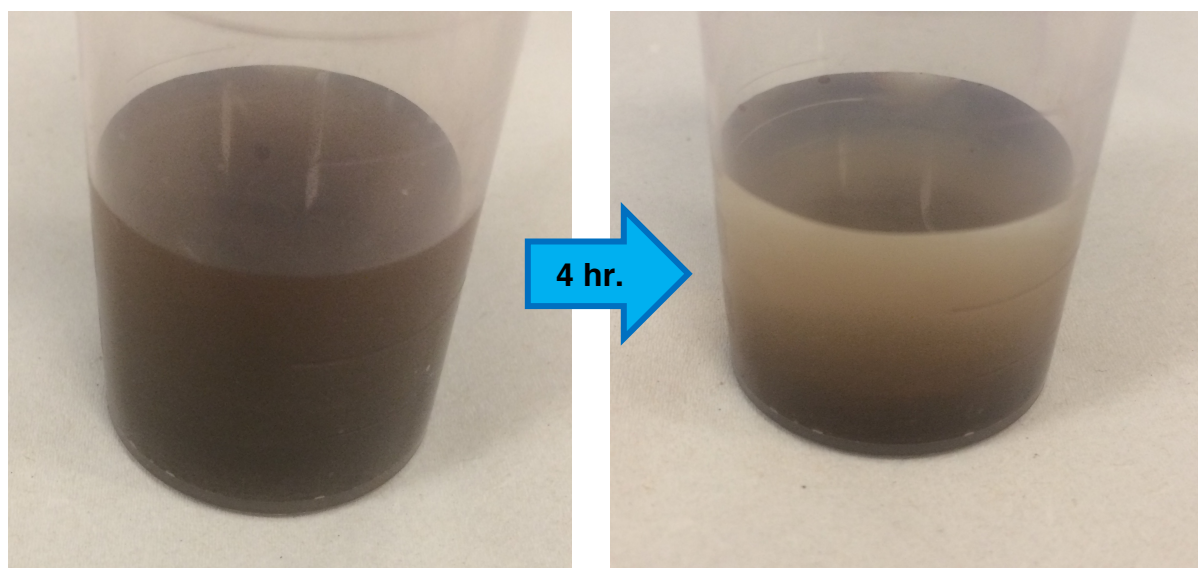


**Figure S27.** Aqueous suspensions of HHCP1 after initial contact and after being left to stand for 4 hr.

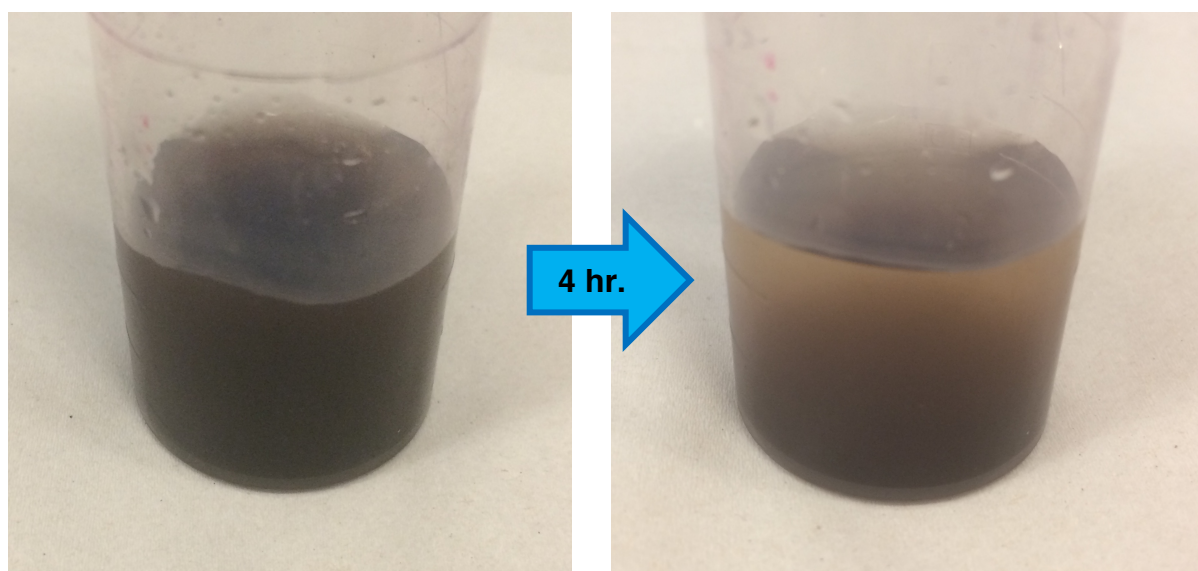


**Figure S28.** Aqueous suspensions of HHCP1-Ca after initial contact and after being left to stand for 4 hr.

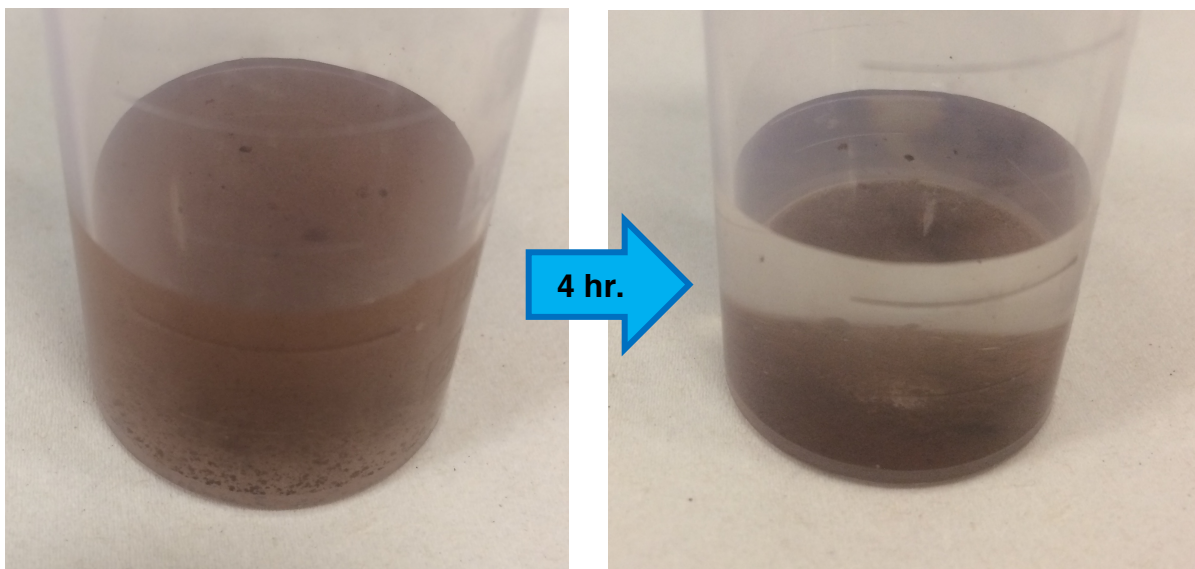


**Figure S29.** Aqueous suspensions of HHCP2 after initial contact and after being left to stand for 4 hr.

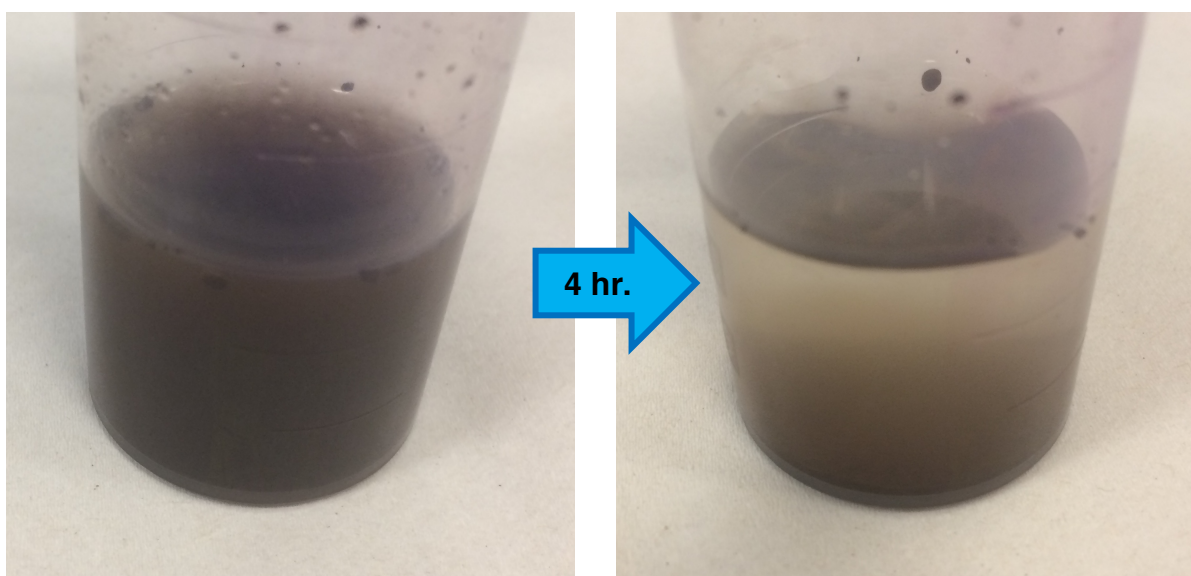


**Figure S30.** Aqueous suspensions of HHCP2-Ca after initial contact and after being left to stand for 4 hr.

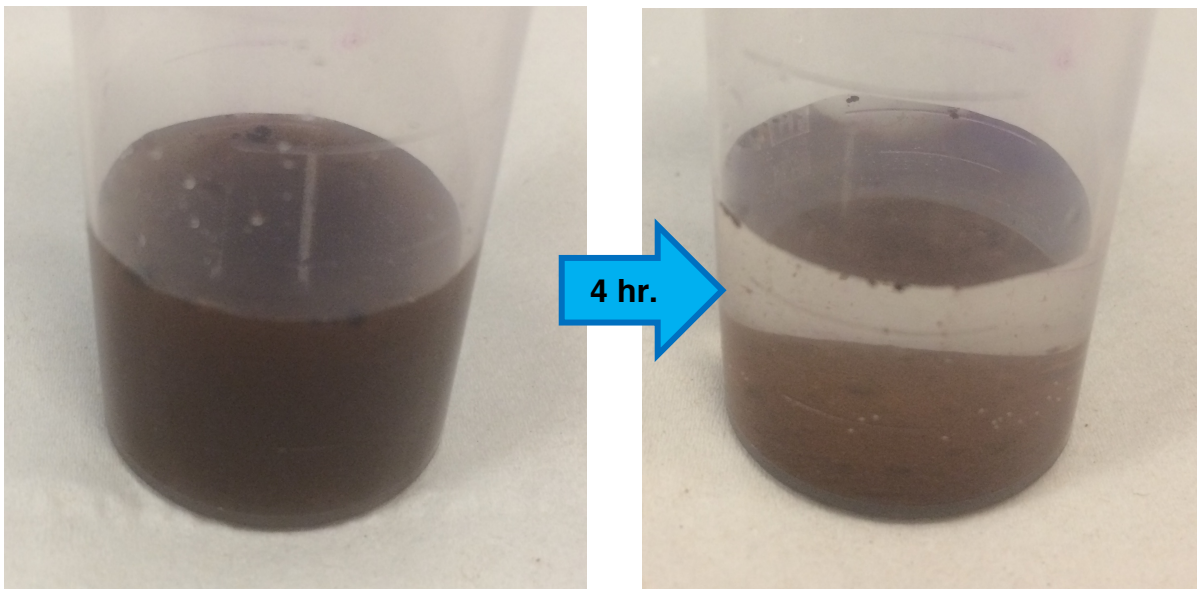


**Figure S31.** Aqueous suspensions of HCP1 after initial contact and after being left to stand for 4 hr.

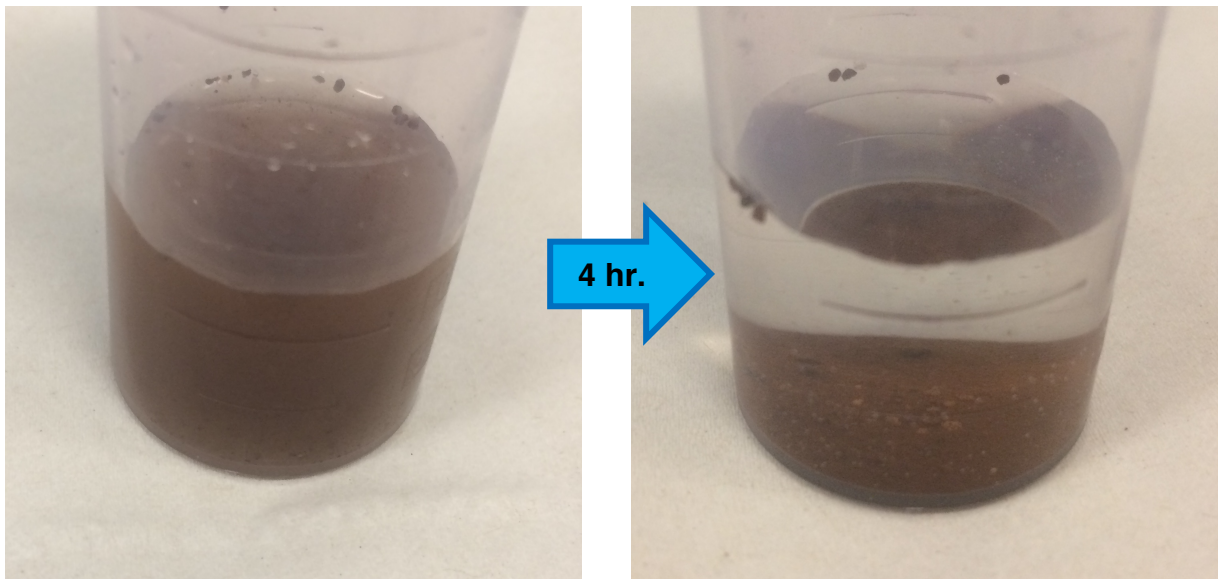


**Figure S32.** Aqueous suspensions of HCP1 +  $\text{Ca}(\text{OH})_2$  after initial contact and after being left to stand for 4 hr.

## Fluoride uptake studies

Static uptake experiments were carried out according to the procedure described in the main article. Equilibrium fluoride uptake capacity ( $q_e$ ) in  $\text{mg}\cdot\text{g}^{-1}$  of the polymers was calculated according to Equation S1:

$$q_e = \frac{(C_1 - C_2)V}{m} \quad (\text{Eqn. S1})$$

Where  $C_1$  is the concentration of fluoride in the sample solution before polymer contact ( $\text{mg}\cdot\text{L}^{-1}$ ),  $C_2$  is the concentration after equilibrium is reached ( $\text{mg}\cdot\text{L}^{-1}$ ),  $V$  is the volume of solution treated (L) and  $m$  is the mass of adsorbent (g).

Fluoride concentration measurements were carried out by ion-selective electrode. A three-point calibration was carried out prior to analysis, using an appropriate range of standards, usually covering two orders of magnitude. These were made by dissolving  $\geq 99.999\%$  NaF, which had been dried in an air-flow oven for a minimum of 24 hr, in deionised water. Recalibration was performed after  $<10$  sample measurements. Each sample contained 50% total ionic strength adjustment buffer (TISAB). For production of TISAB, all reagents were of analytical grade and used without further purification. In a 1 L beaker, 45.0 g NaCl was dissolved in  $\sim 500$  mL deionised water, followed by 4.00 g 1,2-Diaminocyclohexanetetraacetic acid hydrate. 57 mL acetic acid was added and the water volume increased to  $\sim 800$  mL. 5M NaOH was added dropwise, to increase pH to 5.5. The solution was then transferred to a 1 L volumetric flask and solution volume increased to exactly 1 L.

## Assessment of all synthesised networks for fluoride uptake capabilities

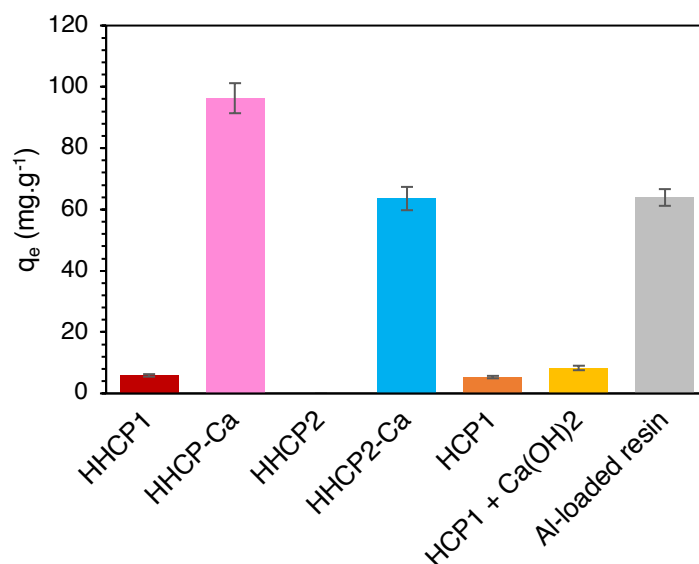


**Figure S33.** Calculated equilibrium uptake capacities for all networks from contact with  $2000\text{ mg}\cdot\text{L}^{-1}$  fluoride solutions, as NaF. Polymer/resin mass = 100 mg. Volume of solution = 25 mL. Contact time = 24 hr.  $T = 18^\circ\text{C}$ .

**Technical note:** The Al-loaded resin was metallated, using the same procedure described in previous work to create a La-loaded resin [9]. The ion-exchange resin used was Puromet™ MTS9501, kindly donated from Purolite, and has an aminomethylphosphonic acid chelating functionality.

## Fluoride uptake as a function of pH and corresponding surface zeta potential

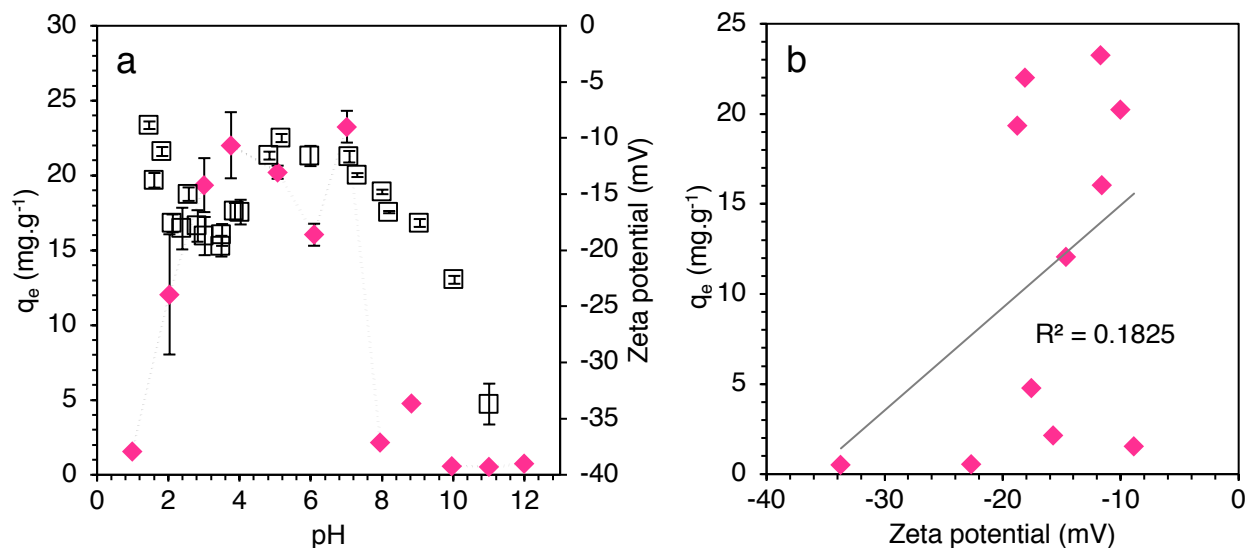


**Figure S34.** (a) Equilibrium fluoride uptake of HHCP1-Ca (◆) over pH range 1-12 with corresponding zeta potential (□) over equivalent pH range. (b) Linear plot of fluoride uptake versus zeta potential for samples where pH was equivalent to  $\pm 0.1$  pH unit. Error bars represent 95% confidence limits from 2 duplicate samples. Polymer mass = 100 mg. Contact solution volume = 25 mL. Initial fluoride concentration =  $100 \text{ mg}\cdot\text{L}^{-1}$ . Contact time = 6 hr.  $T = 18^\circ\text{C}$ .

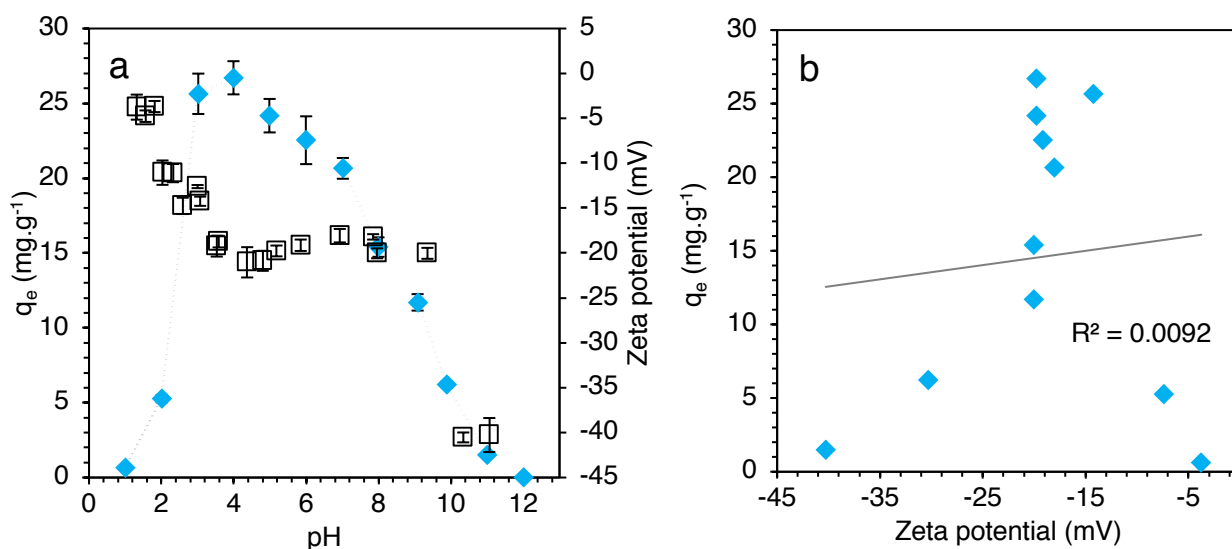


**Figure S35.** (a) Equilibrium fluoride uptake of HHCP2-Ca (◆) over pH range 1-12 with corresponding zeta potential (□) over equivalent pH range. (b) Linear plot of fluoride uptake versus zeta potential for samples where pH was equivalent to  $\pm 0.1$  pH unit. Experimental parameters as per Figure S34.

## Models used to fit isotherm data

### The Langmuir model

The Langmuir isotherm model, (Equation S2) assumes monolayer adsorption over a finite number of degenerate binding sites, with no interaction between adsorbed species.

$$q_e = \frac{q_{\max} K_L C_e}{1 + K_L C_e} \quad (\text{Eqn. S2})$$

In the Langmuir equation,  $q_{\max}$  ( $\text{mg}\cdot\text{g}^{-1}$ ) is the theoretical maximal uptake capacity of the adsorbent.  $K_L$  is a Langmuir Isotherm constant related to the favourability of adsorption.  $C_e$  ( $\text{mg}\cdot\text{L}^{-1}$ ) is the fluoride concentration in solution at equilibria.

### The Freundlich model

The Freundlich isotherm (Equation 3) was originally purely an empirical model. However, it is now commonly quoted as being able to describe multilayer adsorption systems where adsorption sites are heterogeneous [10].

$$q_e = K_F C_e^n \quad (\text{Eqn. S3})$$

$K_F$  and  $n$  are Freundlich isotherm constants.  $K_F$  is a measure of adsorption capacity and  $n$  is a factor of heterogeneity.

### The Temkin model

The Temkin isotherm (Equation S4) has been applied to systems where the heat of adsorption decreases linearly as exchange sites are occupied, as a result of interactions between the sorbate species in solution and on the adsorbent surface [11].

$$q_e = \frac{RT}{b_T} \ln (A_T C_e) \quad (\text{Eqn. S4})$$

$R$  is the ideal gas constant ( $8.314 \text{ J}\cdot\text{K}^{-1}\cdot\text{mol}^{-1}$ ),  $T$  is temperature (K),  $b_T$  is the molar enthalpy of adsorption ( $\text{kJ}\cdot\text{mol}^{-1}$ ) and  $A_T$  is a Temkin isotherm constant ( $\text{L}\cdot\text{g}^{-1}$ ). The term  $\frac{RT}{b_T}$  is often represented by a single constant  $B$ , related to the heat of adsorption.

### The Dubinin-Radushkevich model

The Dubinin-Radushkevich isotherm (Equation S5) assumes the adsorption follows a Gaussian distribution of binding energies is used to determine whether chemisorption, ion-exchange or physisorption dominates the system [12]

$$q_e = q_{\max} e^{-B_D \left[ RT \ln \left( 1 + \frac{1}{C_e} \right) \right]^2} \quad (\text{Eqn. S5})$$

$B_D$  is a D-R isotherm constant ( $\text{mol}^2\cdot\text{J}^2$ ). The mean free energy of sorption  $E_D$  ( $\text{J}\cdot\text{mol}^{-1}$ ) can thus be obtained via Equation S6.

$$E_D = \frac{1}{\sqrt{2B_D}} \quad (\text{Eqn. S6})$$

The model-fitting to the data and subsequent calculation of parameters associated with each isotherm was achieved using non-linear least-squares analysis, using the Microsoft SOLVER programme, according to the method of Billo [13]. The errors associated with the parameters and  $R^2$  values were acquired using Billo's "SolvStat" Excel add-in.

**Table S13.** Key parameters obtained from fitting experimental data from main research article to isotherm models.

Model	Parameter	HHCP1-Ca	HHCP2-Ca
Langmuir	$K_L$	$7.29 \pm 2.80 \times 10^{-4}$	$4.52 \pm 1.00$
	$q_{\max}$ (mg·g <sup>-1</sup> )	$240 \pm 60$	$74.6 \pm 5.4$
	$R^2$	0.946	0.941
Freundlich	$K_F$ (mg·g <sup>-1</sup> )	$0.608 \pm 0.400$	$4.42 \pm 2.00$
	$n$	$1.35 \pm 0.18$	$2.65 \pm 0.48$
	$R^2$	0.912	0.845
Temkin	$A_T$ (L·g <sup>-1</sup> )	$198 \pm 17$	$781 \pm 200$
	$b_T$ (kJ·mol <sup>-1</sup> )	$1.13 \pm 0.07$	$2.86 \pm 0.27$
	$B$	$2.20 \pm 0.13$	$0.867 \pm 0.83$
	$R^2$	0.977	0.939
Dubinin-Radushkevich	$B_D$ (mol <sup>2</sup> ·J <sup>-2</sup> )	$1.74 \pm 0.17 \times 10^{-8}$	$8.21 \pm 1.20 \times 10^{-9}$
	$q_{\max}$ (mg·g <sup>-1</sup> )	$267 \pm 34$	$96.2 \pm 10$
	$E_D$ (kJ·mol <sup>-1</sup> )	$5.36 \pm 0.34$	$7.81 \pm 0.79$
	$R^2$	0.962	0.935

**Table S14.** Comparison on maximum uptake capacity values of polymers compared to other relevant sorbents reported in the literature.

Description of adsorbent	Calculated $q_{\max}$ (mg·L <sup>-1</sup> )	Concentration range (mg·L <sup>-1</sup> )	Reference
HHCP1	$267 \pm 34$	50 - 2000	This work
HHCP2	$96.2 \pm 10$	50 - 2000	This work
La-loaded commercial IX resin	$187 \pm 15$	10 - 1500	[9]
Al-loaded commercial IX resin	12.2	10 - 50	[14]
La-modified activated alumina	6.7	<1 - 20	[15]
SO <sub>4</sub> <sup>2-</sup> doped Fe <sub>3</sub> O <sub>4</sub> /Al <sub>2</sub> O <sub>3</sub> nanoparticles	70.4	2 - 160	[16]
MgAl-CO <sub>3</sub> layered double hydroxide clay	$318 \pm 6$	5 - 2500	[17]
B and N containing conjugated microporous polymer	24	<1 - 50 (estimated from dataset)	[18]
Chitosan-coated perlite	64.1	5 - 25	[19]
Th-complexed bis[2-methacryloyloxy)-ethyl] phosphate polymer	4.32	1 - 10	[20]
Activated alumina	8.27	1 - 20	[21]
MIL-88A (MOF)	40.4	5 - 250	[22]

## Determination of release of OH<sup>-</sup> and Ca<sup>2+</sup> from networks during fluoride uptake

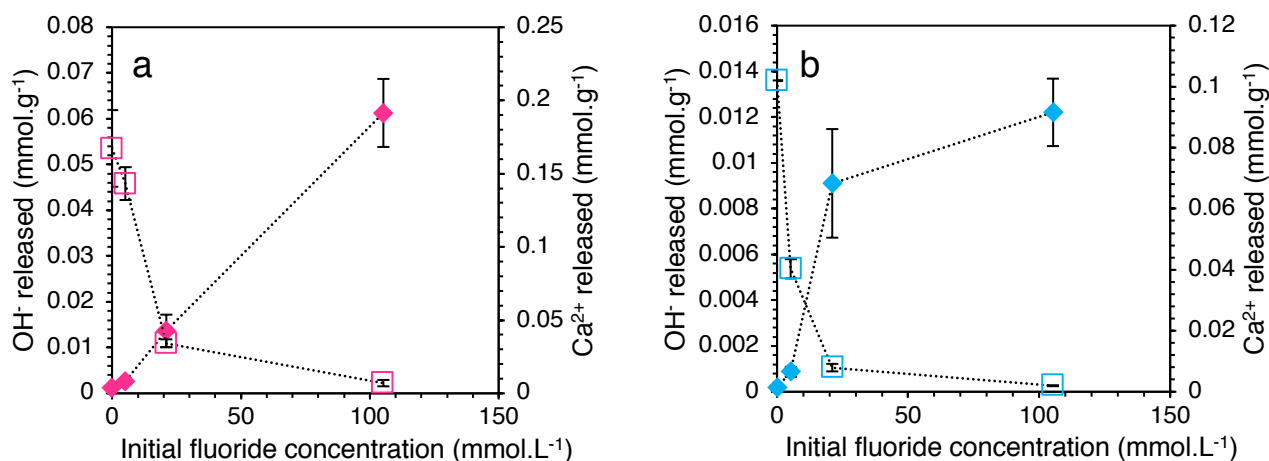


**Figure S36.** Monitoring of quantities of OH<sup>-</sup> (◆) and Ca<sup>2+</sup> (□) released into solution, as a function of initial fluoride solution concentration, during batch equilibrium experiments for (a) HHCP1-Ca and (b) HHCP2-Ca. Polymer mass = 100 mg. Solution volume = 25 mL. T = 18°C.

### Models used to fit static kinetic data

#### The pseudo first-order (PFO) model

The PFO model (Equation S7) is used to describe adsorption data where the uptake behaviour is analogous to a first-order chemical reaction [23]. It is often used to successfully model physisorption mechanisms.

$$q_t = q_e(1 - e^{-k_1 t}) \quad (\text{Eqn. S7})$$

In the PFO model,  $q_t$  is the uptake capacity at a given time,  $t$  is time in minutes and  $k_1$  is the pseudo first-order rate constant in  $\text{min}^{-1}$ .

#### The pseudo second-order (PSO) model

The PSO model (Equation S8) is used to describe adsorption data where the uptake behaviour is analogous to a second-order chemical reaction [24]. It often fits chemisorption uptake data well. However, agreement with this model does not necessarily indicate that the mode of uptake is chemisorption [25].

$$q_t = \frac{k_2 q_e^2 t}{1 + k_2 q_e t} \quad (\text{Eqn. S8})$$

In the PSO model,  $k_2$  is the pseudo second-order rate constant in  $\text{g}\cdot\text{mg}^{-1}\cdot\text{min}^{-1}$ . Other terms are as per the PFO model. Additional parameters may be calculated from the PSO model, using the equations below (S9 and S10).

$$t_{1/2} = \frac{1}{k_2 q_e} \quad (\text{Eqn. S9})$$

$$h_0 = k_2 q_e^2 \quad (\text{Eqn. S10})$$

In these equations,  $t_{1/2}$  is the sorption half-time (min) and  $h_0$  is the initial sorption rate ( $\text{mg}\cdot\text{g}^{-1}\cdot\text{min}^{-1}$ ).

### The Elovich model

This model (Equation S11) may be applied, using a simplification proposed by Chien and Clayton [26].

$$q_t = \frac{1}{\beta} \ln(t) + \frac{1}{\beta} \ln(\alpha\beta) \quad (\text{Eqn. S11})$$

In this model,  $\alpha$  is the initial rate constant ( $\text{mg}\cdot\text{g}^{-1}\cdot\text{min}^{-1}$ ) and  $\beta$  is a desorption constant ( $\text{mg}\cdot\text{g}^{-1}$ ). Agreement with this model is often interpreted to mean that adsorption involves two or three simultaneous first-order reactions [26].

For these three models, fitting to the data and subsequent calculation of associated parameters and errors values was performed using SOLVER, as before.

### The Boyd (film-diffusion) model

This model (Equation S12) considers the transport of the sorbate species through the hydrous film layer surrounding the adsorbent particle [27].

$$\ln(1 - F) = k_{fd} t \quad (\text{Eqn. S12})$$

$F$  is the fractional attainment of equilibrium at time  $t$  and  $k_{fd}$  is the film-diffusion rate constant ( $\text{min}^{-1}$ ). Therefore, in a plot of  $-\ln(1 - C_t/C_i)$  vs  $t$ , a linear gradient would indicate that the uptake rate is controlled by the movement of adsorbate ions within the pores of the resin beads (intra-particle-diffusion). A non-linear gradient would suggest the rate is controlled by the movement of the adsorbate through the hydrous film layer surrounding the adsorbent particles (film-diffusion), or the chemical reaction at the surface [28].

### The intra-particle model

This model (Equation S13) considers the movement of the sorbate species through the pores of the adsorbent particle to the active binding sites [29].

$$q_t = k_{id} t^{1/2} + C \quad (\text{Eqn. S13})$$

In the intra-particle model,  $k_{id}$  is the intra-particle-diffusion rate constant ( $\text{mg}\cdot\text{g}^{-1}\cdot\text{min}^{-1/2}$ ) and  $C$  is a constant relating to the thickness of the adsorbent film layer. In a plot of  $q_t$  vs  $t^{1/2}$ , a linear gradient, passing through the origin, indicates the adsorption is entirely controlled by intra-particle-diffusion [30].

For these two models, fitting to the data and generation of  $R^2$  values was performed using simple linear regression.

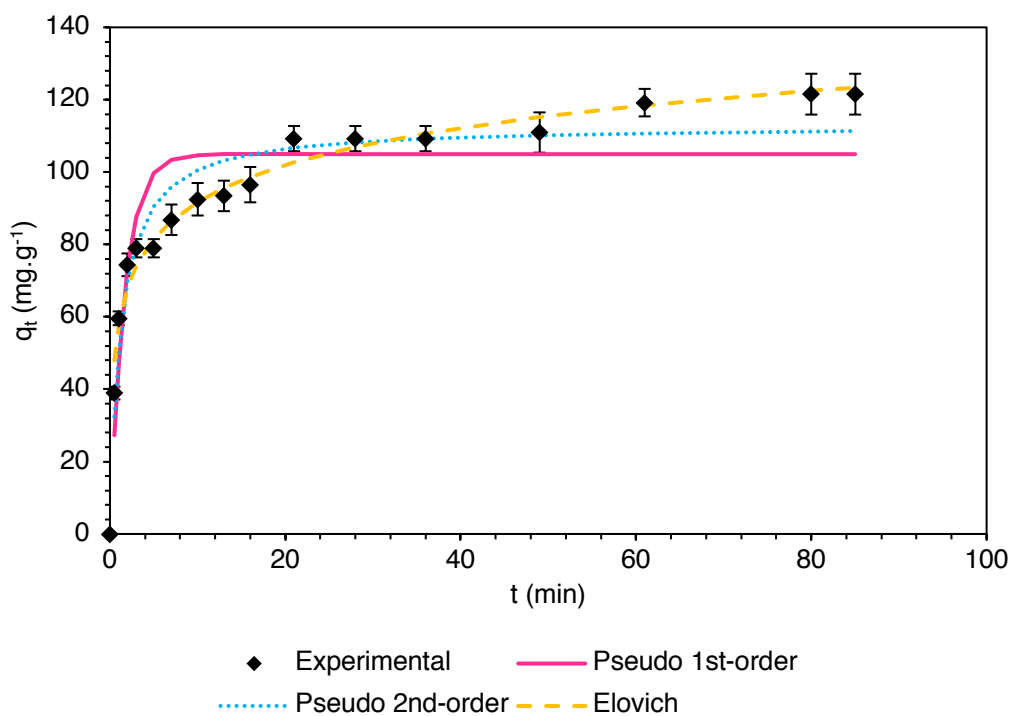


**Figure S37.** Uptake of fluoride over time by HHCP1-Ca and associated fitting to kinetic models. Error bars represent 95% confidence limits from 3 replicate electrode measurements. Polymer mass = 2.00 g. Contact solution initial volume = 500 mL. Initial fluoride concentration = 2000  $\text{mg}\cdot\text{L}^{-1}$ .  $T = 18^\circ\text{C}$ .

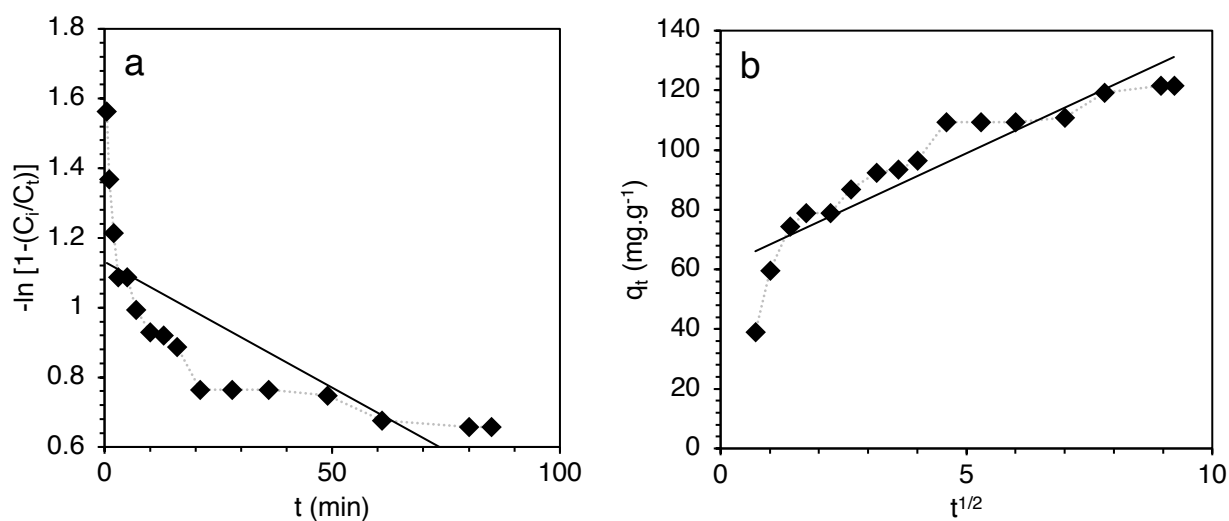


**Figure S38.** Fitting of the above uptake data to (a) film diffusion and (b) intra-particle diffusion models.

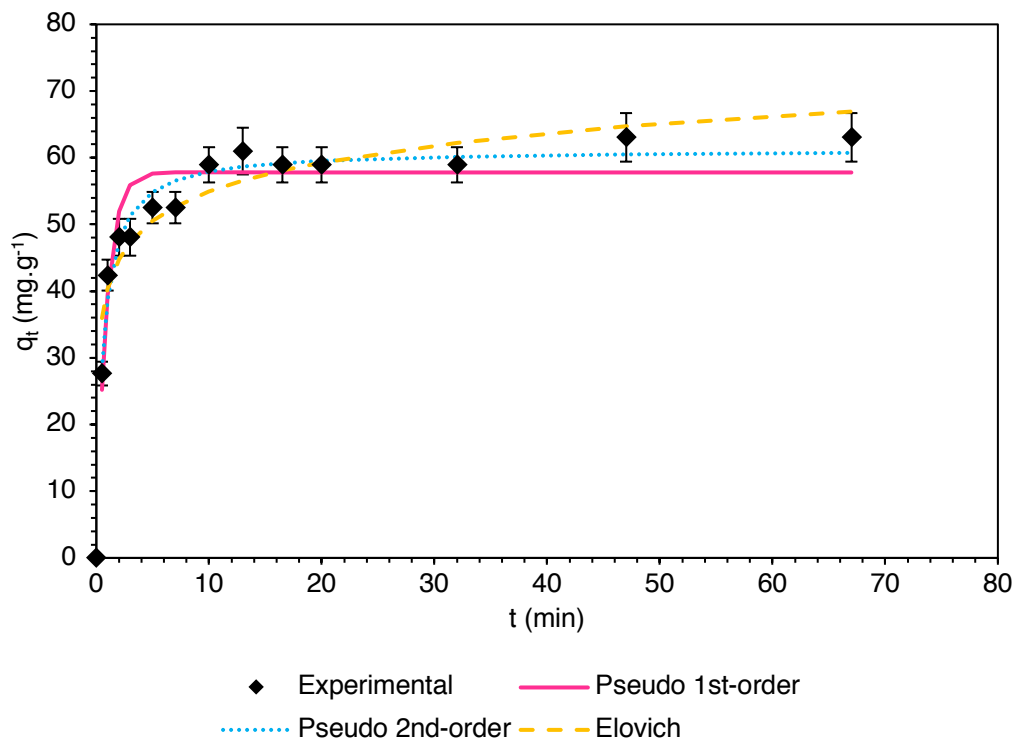


**Figure S39.** Uptake of fluoride over time by HHCP2-Ca and associated fitting to kinetic models. Error bars represent 95% confidence limits from 3 replicate electrode measurements. Polymer mass = 2.00 g. Contact solution initial volume = 500 mL. Initial fluoride concentration = 2000  $\text{mg}\cdot\text{L}^{-1}$ .  $T = 18^\circ\text{C}$ .

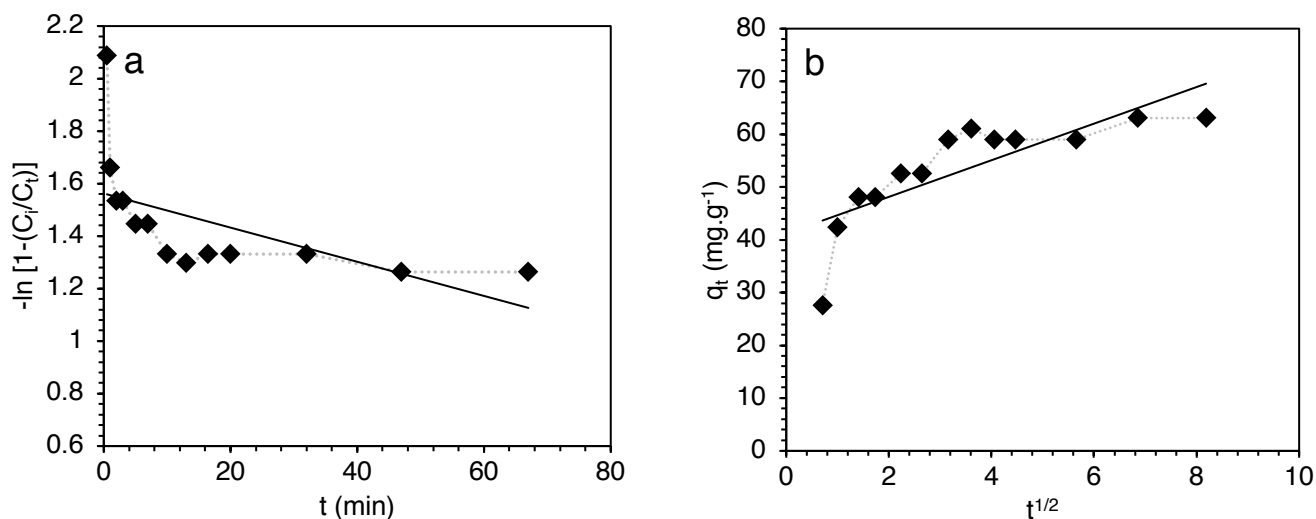


**Figure S40.** Fitting of the above uptake data to (a) film diffusion and (b) intra-particle diffusion models.

**Table S15.** Extracted parameters from model-fitting to static kinetic data for both networks.

Model	Parameter	HHCP1-Ca	HHCP2-Ca
PFO	$k_1$ (min <sup>-1</sup> )	0.602 ± 0.13	1.15 ± 0.17
	$q_e$ (mg·g <sup>-1</sup> )	105 ± 4	57.8 ± 17
	$R^2$	0.787	0.844
PSO	$k_2$ (g·mg <sup>-1</sup> ·min <sup>-1</sup> )	7.15 ± 1.4 (x 10 <sup>-3</sup> )	2.81 ± 0.36 (x 10 <sup>-2</sup> )
	$q_e$ (mg·g <sup>-1</sup> )	113 ± 3	61.3 ± 1.0
	$h_0$ (mg·g <sup>-1</sup> ·min <sup>-1</sup> )	91.2 ± 18	105 ± 14
	$t_{1/2}$ (min)	1.24 ± 0.24	0.581 ± 0.076
	$R^2$	0.905	0.946
Elovich	$\alpha$ (mg·g <sup>-1</sup> ·min <sup>-1</sup> )	3.84 ± 1.0 (x 10 <sup>-2</sup> )	0.196 ± 0.039
	$\beta$ (mg·g <sup>-1</sup> )	1290 ± 60	3000 ± 350
	$R^2$	0.971	0.872
Film diffusion	$R^2$	0.592	0.336
Intra-particle diffusion	$R^2$	0.829	0.627

### Notes

For both networks, the plot of  $-\ln(1-C_t/C_i)$  vs  $t$  does not yield a linear gradient. The plot of  $q_t$  vs  $t^{1/2}$  also does not yield a linear gradient. Collectively, this indicates that intra-particle-diffusion is not the rate-determining step and that film-diffusion or chemical reaction is more likely to be rate-controlling.

### Dynamic breakthrough data

The fluoride breakthrough data for columns loaded with HHCP1-Ca and HHCP2-Ca was fitted with the empirical Dose-Response model (Equations S14 and S15) [31].

$$\frac{C}{C_i} = 1 - \frac{1}{1 + \left(\frac{V_{\text{eff}}}{b}\right)^a} \quad (\text{Eqn. S14})$$

$$q_0 = \frac{bC_i}{m} \quad (\text{Eqn. S15})$$

Here,  $C$  is the concentration of fluoride in the effluent at a given point,  $C_i$  is the concentration of fluoride in the inlet stream,  $V_{\text{eff}}$  is the volume of solution eluted from the column (mL),  $a$  and  $b$  are constants of the Dose-Response model,  $q_0$  is the theoretical maximum uptake capacity of the resin in a dynamic environment (mg·g<sup>-1</sup>) and  $m$  is the dry mass of resin (g).

Fitting to the data and subsequent calculation of associated parameters and errors values was performed using SOLVER, as before.

**Table S16.** Parameters returned from fitting dynamic breakthrough data for HHCP1-Ca and HHCP2-Ca to Dose-Response model. Polymer mass = 1.30 g. Inlet [F<sup>-</sup>] = 2000 mg·L<sup>-1</sup>. Flow rate = 2.75 mL·hr<sup>-1</sup>. T = 18°C.

Parameter	HHCP1-Ca	HHCP2-Ca
$a$	4.96 ± 0.20	3.06 ± 0.06
$b$	58.9 ± 0.5	22.0 ± 0.2
$q_0$ (mg·g <sup>-1</sup> )	95.8 ± 0.8	58.4 ± 0.4
$R^2$	0.991	0.999

## Selectivity and competition effects via ion chromatography analysis

A solution was made up, containing 1 mM of 8 common anions, as their Na salts ( $F^-$ ,  $Cl^-$ ,  $NO_3^-$ ,  $Br^-$ ,  $PO_4^{3-}$ ,  $SO_4^{2-}$ ,  $I^-$  and  $CO_3^{2-}$ ). This solution was contacted by HHCP1-Ca and HHCP2-Ca, as described in the main article. The fluoride uptake was compared to control samples of 1 mM fluoride only. Pre-contact and post-contact anion concentrations were determined by ion chromatography, as described in the main article. The instrument was calibrated with solutions of 1-10  $mg \cdot L^{-1}$  of the relevant anions, which were diluted from 1000  $mg \cdot L^{-1}$  analytical standards, purchased from Fisher Scientific. The equilibrium uptake capacity for the various anions ( $q_e$ ) in  $mmol \cdot g^{-1}$  was calculated using the procedure described in the main research article. The distribution coefficient ( $K_D$ ) for each anion was calculated as follows (Equation S16):

$$K_D = \frac{[\overline{X^-}]}{[X^-]} \quad (\text{Eqn. S16})$$

where  $[\overline{X^-}]$  is the concentration of anion immobilized by the polymer ( $mmol \cdot g^{-1}$ ) and  $[X^-]$  is the concentration remaining in solution at equilibrium ( $mmol \cdot mL^{-1}$ ).

The separation factor (S.F.) is then calculated from Equation S17:

$$S.F._{(X/Y)} = \frac{K_{d(X)}}{K_{d(Y)}} \quad (\text{Eqn. S17})$$

Where X is the ion of interest and Y is a competing ion.

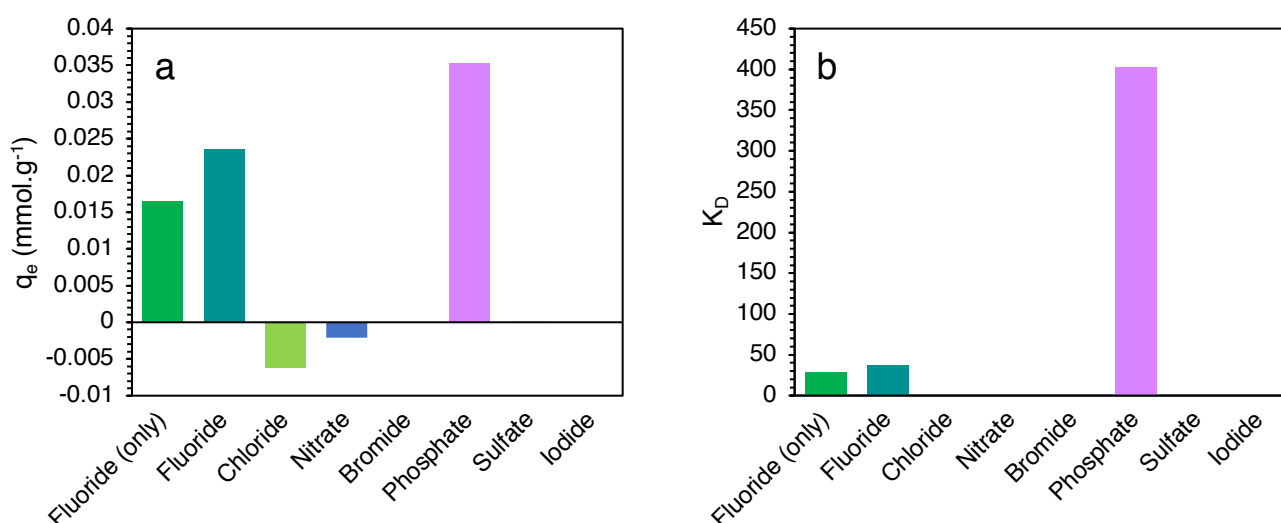


**Figure S41.** (a) Uptake of common anions by HHCP1-Ca. (b)  $K_D$  values for each anion. Polymer mass = 100 mg. Contact solution volume = 25 mL. Initial concentration of anions = 1.00 mM. Contact time = 6 hr.  $T = 18^\circ C$ .

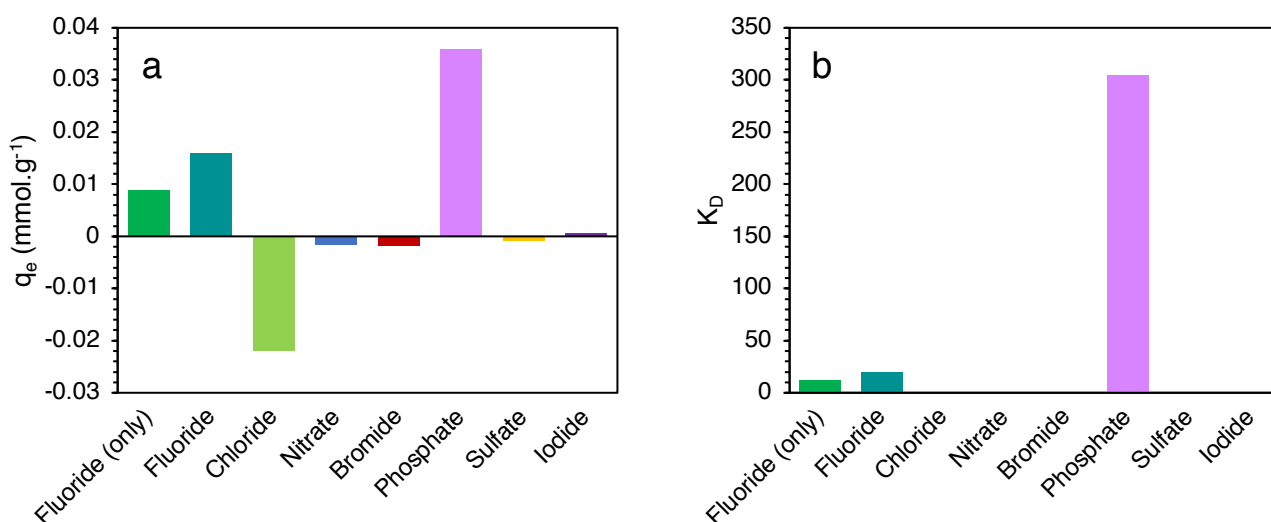


**Figure S42.** (a) Uptake of common anions by HCCP2-Ca. (b)  $K_D$  values for each anion. Polymer mass = 200 mg. Contact solution volume = 10 mL. Initial concentration of anions = 1.00 mM. Contact time = 6 hr.  $T = 18^\circ\text{C}$ .

The relevant S.F.s for fluoride vs the competing anions is shown in Table S17.

**Table S17.** Calculated S.F.s of HHCP1-Ca and HHCP2-Ca from  $K_D$  data for fluoride with respect to competing anions.  $\text{Cl}^-$  and  $\text{NO}_3^-$  are not presented as they were released into solution during the equilibrium process.

Network	Separation Factor ( $F^-/\text{competing anion}$ )			
	$\text{Br}^-$	$\text{PO}_4^{3-}$	$\text{SO}_4^{2-}$	$\text{I}^-$
HHCP1-Ca	>10000	$9.18 \times 10^{-2}$	1130	>10000
HHCP2-Ca	>10000	$6.40 \times 10^{-2}$	>10000	23.5

### Defluoridation performance of the polymers over several cycles

Regeneration of HHCP1-Ca and HHCP2-Ca was attempted, using the procedures described in the main article. The fluoride uptake capacities of the networks, after each desorption/adsorption cycle, were measured.

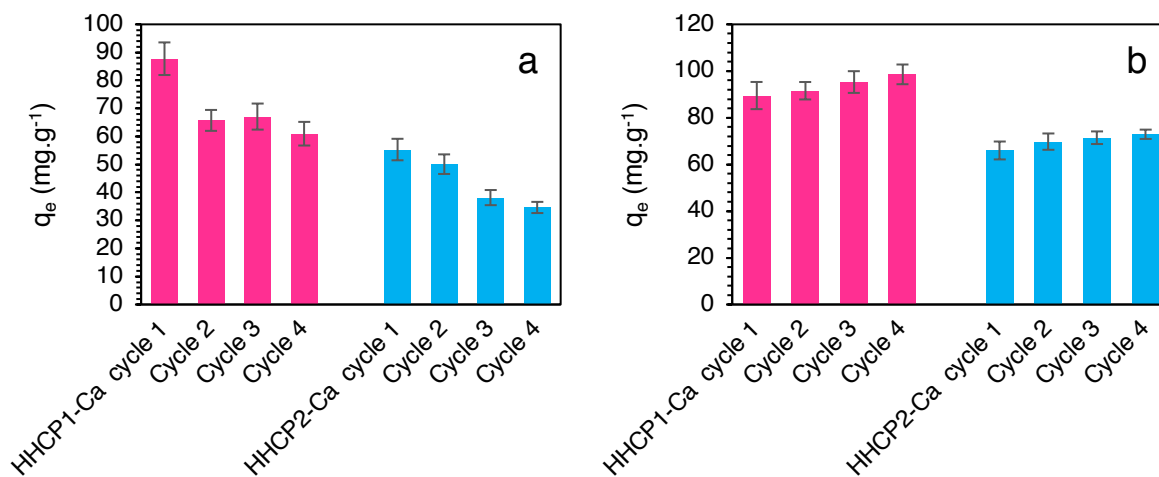


**Figure S43.** Equilibrium uptake capacity of HHCP1-Ca and HHCP2-Ca over repeated cycles of fluoride-loading and desorption/regeneration attempts. **(a)** Treatment with 1 M NaOH. **(b)** Treatment with 1 M HNO<sub>3</sub>, then reloading with Ca<sup>2+</sup>. Polymer mass = 100 mg. Contact solution volume = 25 mL. Initial fluoride concentration = 2000 mg·L<sup>-1</sup>. Contact time = 6 hr. T = 18°C.

**Note:** “cycle 1” refers to the as-synthesised polymers, prior to any regeneration attempt.

## References

- [1] R. Dawson, L.A. Stevens, T.C. Drage, C.E. Snape, M.W. Smith, D.J. Adams, A.I. Cooper, Impact of Water Coadsorption for Carbon Dioxide Capture in Microporous Polymer Sorbents, *Journal of The American Chemical Society*, **134** (2012) 10741-10744.
- [2] R.H. Schlosberg, C.G. Scouten, Organic-chemistry of calcium - formation and pyrolysis of hydroxycalcium phenoxides, *Energy & Fuels*, **2** (1988) 582-585.
- [3] F.A. Andersen, L. Brecevic, Infrared-spectra of amorphous and crystalline calcium-carbonate, *Acta Chemica Scandinavica*, **45** (1991) 1018-1024.
- [4] M. Galvan-Ruiz, J. Hernandez, L. Banos, J. Noriega-Montes, M.E. Rodriguez-Garcia, Characterization of Calcium Carbonate, Calcium Oxide, and Calcium Hydroxide as Starting Point to the Improvement of Lime for Their Use in Construction, *Journal of Materials in Civil Engineering*, **21** (2009) 694-698.
- [5] M. Ni, B.D. Ratner, Differentiation of Calcium Carbonate Polymorphs by Surface Analysis Techniques – An XPS and TOF-SIMS study, *Surface Interface Analysis*, **40** (2008) 1356-1361.
- [6] D. Steele, E.R. Lippincott, The Crystal and Solution Vibrational Spectra of Biphenyl, *Journal of Molecular Spectroscopy*, **6** (1961) 238-264.
- [7] R. Ullah, I. Ahmad, Y. Zheng, Fourier Transform Infrared Spectroscopy of Bisphenol A, *Journal of Spectroscopy*, (2016) 1-5.
- [8] R. Vinodh, P. Hemalatha, M. Ganesh, M.M. Peng, A. Abidov, M. Palanichamy, W.S. Chab, H.T. Jang, Novel microporous hypercross-linked conjugated quinonoid chromophores with broad light absorption and CO<sub>2</sub> sorption characteristics, *RSC Advances*, **4** (2014) 3668-3674.
- [9] T. Robshaw, S. Tukra, D.B. Hammond, G.J. Leggett, M.D. Ogden, Highly efficient fluoride extraction from simulant leachate of spent potlining via La-loaded chelating resin. An equilibrium study, *Journal of Hazardous Materials*, **361** (2019) 200-209.
- [10] K.Y. Foo, B.H. Hameed, Insights into the modeling of adsorption isotherm systems, *Chemical Engineering Journal*, **156** (2010) 2-10.

- [11] M. Eriksson, I. Lundstrom, L.G. Ekedahl, A model of the Temkin isotherm behavior for hydrogen adsorption at Pd-SiO<sub>2</sub> interfaces, *Journal of Applied Physics*, **82** (1997) 3143-3146.
- [12] A.A. Inyinbor, F.A. Adekola, G.A. Olatunji, Kinetics, isotherms and thermodynamic modeling of liquid phase adsorption of Rhodamine B dye onto *Raphia hookerie* fruit epicarp, *Water Resources and Industry*, **15** (2016) 14-27.
- [13] E.J. Billo, *Excel for Chemists: A Comprehensive Guide*, 3rd ed., John Wiley, Hoboken, New Jersey, 2004.
- [14] D.B. Bhatt, P.R. Bhatt, H.H. Prasad, K.M. Popat, P.S. Anand, Removal of fluoride ion from aqueous bodies by aluminium complexed amino phosphonic acid type resins, *Indian Journal of Chemical Technology*, **11** (2004) 299-303.
- [15] J.M. Cheng, X.G. Meng, C.Y. Jing, J.M. Hao, La<sup>3+</sup>-modified activated alumina for fluoride removal from water, *Journal of Hazardous Materials*, **278** (2014) 343-349.
- [16] L.Y. Chai, Y.Y. Wang, N. Zhao, W.C. Yang, X.Y. You, Sulfate-doped Fe<sub>3</sub>O<sub>4</sub>/Al<sub>2</sub>O<sub>3</sub> nanoparticles as a novel adsorbent for fluoride removal from drinking water, *Water Research*, **47** (2013) 4040-4049.
- [17] L. Lv, J. He, M. Wei, D.G. Evans, Z.L. Zhou, Treatment of high fluoride concentration water by MgAl-CO<sub>3</sub> layered double hydroxides: Kinetic and equilibrium studies, *Water Research*, **41** (2007) 1534-1542.
- [18] Z.P. Li, H. Li, H. Xia, X.S. Ding, X.L. Luo, X.M. Liu, Y. Mu, Triarylboron-Linked Conjugated Microporous Polymers: Sensing and Removal of Fluoride Ions, *Chemistry-A European Journal*, **21** (2015) 17355-17362.
- [19] Y. Vijaya, M.V. Subbaiah, A.S. Reddy, A. Krishnaiah, Equilibrium and kinetic studies of fluoride adsorption by chitosan coated perlite, *Desalination and Water Treatment*, **20** (2010) 272-280.
- [20] N. Thakur, S.A. Kumar, D.N. Wagh, S. Das, A.K. Pandey, S.D. Kumar, A.V.R. Reddy, Matrix supported tailored polymer for solid phase extraction of fluoride from variety of aqueous streams, *Journal of Hazardous Materials*, **201** (2012) 193-201.
- [21] R. Leyva-Ramos, N.A. Medellin-Castillo, A. Jacobo-Azuara, J. Mendoza-Barron, L.E. Landin-Rodriguez, J.M. Martinez-Rosales, A. Aragon-Pina, Fluoride removal from water solution by adsorption on activated alumina prepared from pseudo-boehmite, *Journal of Environmental Engineering Management*, **18** (2008) 301-309.
- [22] F. Ke, G. Luo, P.R. Chen, J. Jiang, Q.Y. Yuan, H.M. Cai, C.Y. Peng, X.C. Wan, Porous metal-organic frameworks adsorbents as a potential platform for defluoridation of water, *Journal of Porous Materials*, **23** (2016) 1065-1073.
- [23] S. Lagergren, Theorie der sogenannten adsorption gelosterstoffe, *Svenska Vetenskapsakademiens Handlingar*, **24** (1898) 1-39.
- [24] G. Blanchard, M. Maunaye, G. Martin, Removal of heavy metals from waters by means of natural zeolites, *Water Research*, **18** (1984) 1501-1507.
- [25] H.N. Tran, S.J. You, A. Hosseini-Bandegharai, H.P. Chao, Mistakes and inconsistencies regarding adsorption of contaminants from aqueous solutions: A critical review, *Water Research*, **120** (2017) 88-116.
- [26] S.H. Chien, W.R. Clayton, Application of Elovich equation to the kinetics of phosphate release and sorption in soils, *Soil Science Society of America Journal*, **44** (1980) 265-268.
- [27] G.E. Boyd, A.W. Adamson, L.S. Myers Jr., The Exchange Adsorption of Ions from Aqueous Solutions by Organic Zeolites. 11. Kinetics, *Journal of The American Chemical Society*, **69** (1947) 2836-2848.
- [28] T.J. Robshaw, R. Dawson, K. Bonser, M.D. Ogden, Towards the implementation of an ion-exchange system for recovery of fluoride commodity chemicals. Kinetic and dynamic studies, *Chemical Engineering Journal*, **367** (2019) 149-159.
- [29] W.J. Weber, J.C. Morris, Kinetics of Adsorption on Carbon from Solution, *Journal of The Sanitary Engineering Division*, **89** (1963) 31-60.

- [30] S.E. Pepper, K.R. Whittle, L.M. Harwood, J. Cowell, T.S. Lee, M.D. Ogden, Cobalt and nickel uptake by silica-based extractants, *Separation Science and Technology*, **53** (2018) 1552-1562.
- [31] G.Y. Yan, T. Viraraghavan, M. Chen, A new model for heavy metal removal in a biosorption column, *Adsorption Science and Technology*, **19** (2001) 25-43.